d/Collection

Functional electrolytes to improve electrochemical properties of cathodes and anodes in Na ion batteries

Jun Yeong Jang

Department of Energy Engineering,

(Battery Science and Technology)

Graduate School of UNIST

2015

Functional electrolytes to improve electrochemical properties of cathodes and anodes in Na ion batteries

Jun Yeong Jang

Department of Energy Engineering,

(Battery Science and Technology)

Graduate School of UNIST

2015

Functional electrolytes to improve electrochemical properties of cathodes and anodes in Na ion batteries

A thesis

submitted to the Graduate School of UNIST
in partial fulfillment of the
requirements for the degree of
Master of Science

Jun Yeong Jang

08. 21. 2015

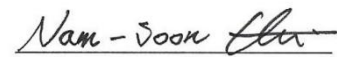Approved by

Major Advisor
Nam-Soon Choi

Functional electrolytes to improve electrochemical properties of cathodes and anodes in Na ion batteries

Jun Yeong Jang

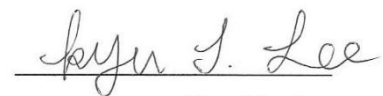This certifies that the thesis of Jun Yeong Jang is approved.

08.21.2015 of submisson

Signature

Nam-Soon Choi (signature)

Thesis supervisor : Nam-Soon Choi

Signature

Kye Tae Lee (signature)

Kye Tae lee

Signature

(signature)

SooJin Park

Abstract

As increasing importance of environment and demand of energy resources, energy devices have attracted a great deal of attention as facilitating smart grid system in society. Especially, large-scale electric energy storage (EES) which can store the electricity during times of excess production and release the electrical energy to the grid is reasonable way to save the energy resources. The Li-ion batteries which are one of successful energy devices show the possibility to application. However, the cost in large-scale ESS is the key issue for application because the cost of Li materials continuously increased.

Recently, Na-ion batteries have been introduced as a promising candidate for next-generation battery systems because the natural abundance of Na resources. The Na materials have high benefit of the cost and it seem to suitable for large-scale ESS. Moreover, Na ion can easily apply Li-battery system due to the similarities with Li. Although Na-ion battery has many advantages for ESS, the large ionic size of sodium make it difficult to application.

In this work, I demonstrate key aspects of the electrolyte formulation and additives to afford high electrochemical performances of $Na_4Fe_3(PO_4)_2(P_2O_7)$ cathode and Sn_4P_3 anodes for Na-ion batteries. In the case of cathode, electrolytes are usually decomposed on electrode due to the high voltage and directly affect the electrochemical performance of cathode. However, I proposed that EC/PC-based electrolyte not only endure electrochemical decomposition in high voltage but also stable against the highly reactive Na metal.

In case of anode, severe volume changes of the metallic anode by Na insertion and extraction cause cracking of the anode particles and lead to a continuous solid electrolyte interphase (SEI)-filming process on the exposed active surface of the anode. In Sn_4P_3, my investigation revealed that the FEC additive makes a resistive NaF-based SEI controlling the formation of $Na_{15}Sn_4$ phase with severe volume expansion and the TMSP additive effectively eliminated HF from the FEC decomposition to mitigate the formation of a large fraction of NaF and build up more stable and robust SEI layers.

Furthermore, I demonstrate the surface chemistry of cathode and anode by using various analyses. This research can contribute to understand the interfacial characteristics and electrochemical reactions for Na-ion batteries.

Contents

List of figures

Figure 3-16. Electrochemical impedance spectra of Sn_4P_3 anodes (a) before and (b) after full sodiation in the baseline, FEC-added, and FEC+TMSP-added electrolyte

CHAPTER I

Introduction

1.1 The Na-ion batteries

1-1-1. Toward energy devices

As industry and technology has been developed in whole society, the increasing demand for powering systems has been grown. From the demand for energy, energy storage devices become key issues to solve resource problem which is short of oil. Moreover, fossil fuel should be replaced as eco-friendly energy to reduce gas emission or pollution of environment.

In the future, smart grid systems which utilize discontinuous energy flow from energy sources should be suitable solution for energy shortage and environment. Especially, electrochemical energy devices are one of the core technologies to facilitate smart grid system. For several decades, many researcher and engineer has absorbed in development of inexpensive and renewable energy devices. In portable devices, Lithium-ion batteries (LIBs) have been successfully commercialized rechargeable batteries which convert chemical energy to electric energy.[1-3] Nowadays, LIBs is required to high energy and high power density for electric vehicles (EVs) and energy storage system (ESS). Therefore, the area of LIBs has come to be one of the most challenging, interesting and promising energy storage systems to replace fossil fuels.
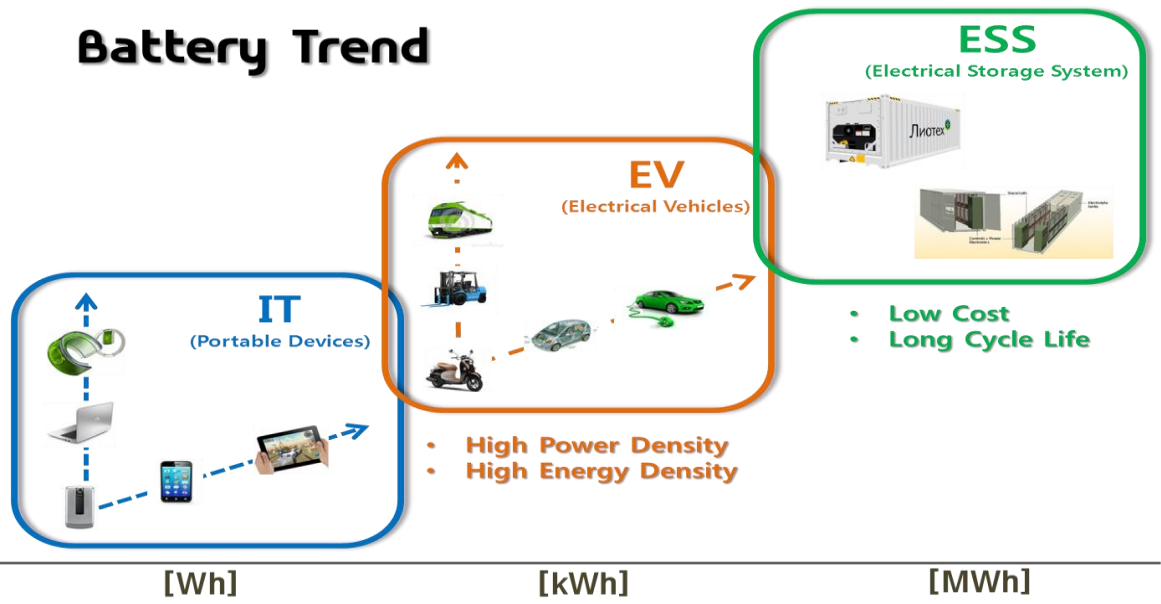
Figure 1-1. Battery trend for future application
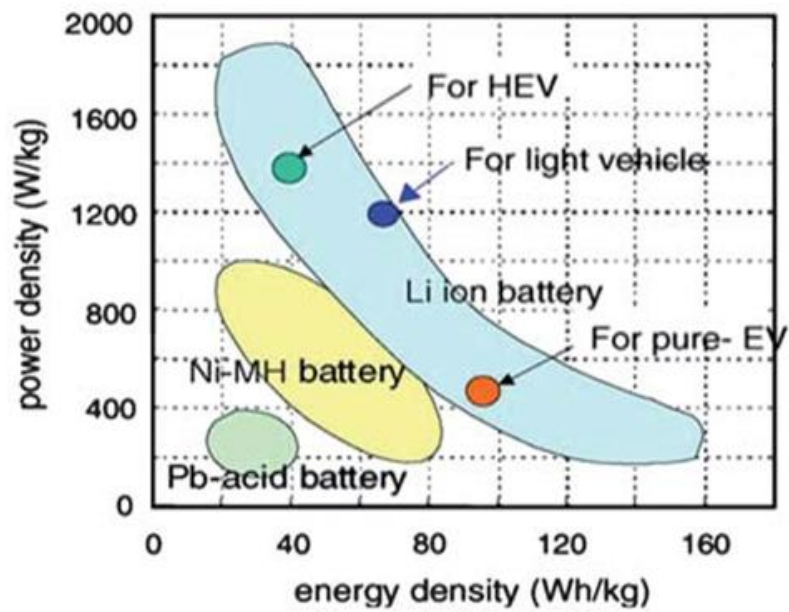
Figure 1-2. Demand of batteries for various applications.[3]

1-1-2. The introduction of rechargeable battery

The battery is energy devices which can convert chemical to electrical energy. The batteries are composed of electrode, electrolyte and separator. The principle of batteries has reaction process which has reduction and oxidation at electrode. As battery has two electrical path ways, electron can move through external circuit and ions move through electrolyte. When batteries are charged, ions and electrons move from cathode to anode. When batteries are discharged, ions and electron move opposite direction of charging process.[4]

Lithium ion batteries (LIBs) are one of the commercialized batteries in portable devices. Lithium has low molecular weight, redox potential (-3.04V vs SHE) and low ionic radius. This unique property of lithium can be chosen as electrochemical sources because these can achieve high energy density in batteries.[5]

The lithium ion batteries are composed of anode, cathode, electrolyte and separator. The cathode of commercial LIBs is $LiCoO_2$ which has lithium sources and anode is graphite which can be intercalated by lithium sources. Cathode and anode are separated to inhibit physical contact. When batteries have charge and discharge process, electrolyte can make lithium ion pathway move between cathode and anode. Lastly, separators keep a cathode apart from anode physically for safety and current flow. Separator which has porous structure makes it possible that lithium move through the electrolyte. The component of LIBs highly related to electrochemical performance of battery. When researcher consider to design batteries, it should be improved each component step by step.

In case of cathode, surface coating or transition metal doping has been great attention to improve performance.[6-7] For example, Al_2O_3 can prevent the cobalt dissolution during cycling and result in improve structural stability.[8-9] In case of anode, promising anode such as conversion and alloy materials has been reported to improve capacity. Especially, Si seems to attractive materials because it has high specific capacity (~4200mAh/g). However, the severe volume expansion of Si during cycling cause mechanical failure and show drastic capacity fading. To solve this problem, carbon coating[10] or making porous structure[11] has been reported as buffer affect during cycling. In addition, the functional binder which is role of holding active materials on the current collector has been introduced to mitigate volume expansion and mechanical failure.[12-14] It is clearly shown that enhancement of cycle performance of silicon anode.

Nowadays, LIBs are facing to challenge for appying electric vehicles (EV), hybrid electric vehicles (HEV) and plug-in hybrid electric vehicle (PHEV). It should be needed for future LIBs that improve density and high capacity and high power density.
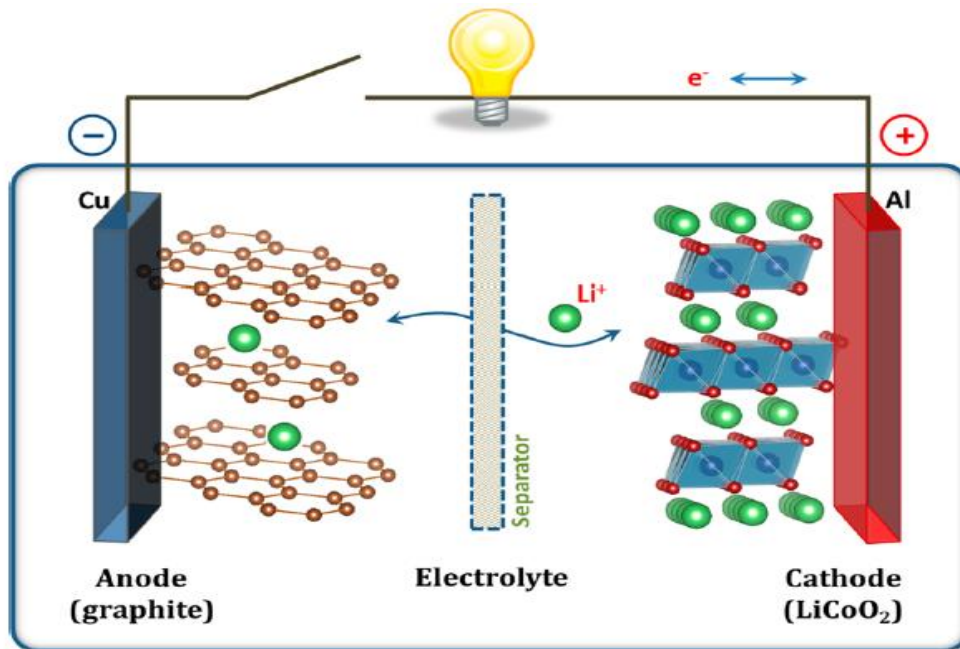
Figure 1-3. Schematic of Li ion battery system.[5]

1-1-3. The characteristics of Na-ion batteries

With development of industry and technology, renewable energy sources such as wind and large-scale electric storage systems have been received great attention. Especially, electric energy storage (EES) is one of promising systems to store the electricity during times of excess production and release the electrical energy to the grid. These systems integrate varying energy sources and society. To achieve successful EES, the battery technology is most important and face to challenging which is cost, energy density and long cycle life.

Although lithium ion batteries are already commercialized in portable devices, the price of lithium sources is rapidly increased due to low abundance in earth crust. It is sure that real application of EES highly related to cost and the price of lithium should be considered. Therefore sodium-ion batteries (NIBs) have been great deal of attention for large scale electric energy storage because of low cost compared to lithium-ion batteries. The price of sodium carbonate is about 150$/ton which is much lower than lithium (~5000$/ton).[15] Moreover, sodium has similarity with lithium because they are located in same group of periodic table. It has convenience to apply lithium battery systems.[16-19]

However, Na ion batteries have many critical issues that should be solved for application. First, Na ion has larger in ionic radius than Li ions, which this is difficult for Na ions to be reversibly inserted into and extracted from host materials. Especially, sodium ion cannot intercalate to graphite anode which is used in commercialized LIBs. For this reason, sodium ion batteries should be needed to find alternative anode. Second, gravimetric energy density of SIBs is lower than LIBs because molecular weight of sodium ion (23g/mol) is higher than lithium ion (6.9g/mol). Lastly, sodium (-2.71V vs SHE) is less reducing than lithium (-3.04V vs SHE). This mean that energy density of SIBs has slightly lower than LIBs.

Although Na-ion battery has a long way to go application, it has reported a number of new materials recently and followed performance of Li ion batteries. Therefore, it is a promising system as alternative for Li-ion batteries due to much lower price and abundance of sodium, and its similarity with lithium.

	Lithium (Li)	Sodium (Na)
Cation radius (Å)	0.76	1.06
Atomic weight	6.9g/mol	23g/mol
SHE (V)	-3.04	-2.71
Cost (carbonates)	$5000/ton	$150/ton
Capacity (mAh/g)	3829	1165

Figure 1-4. Characteristics of Lithium and sodium
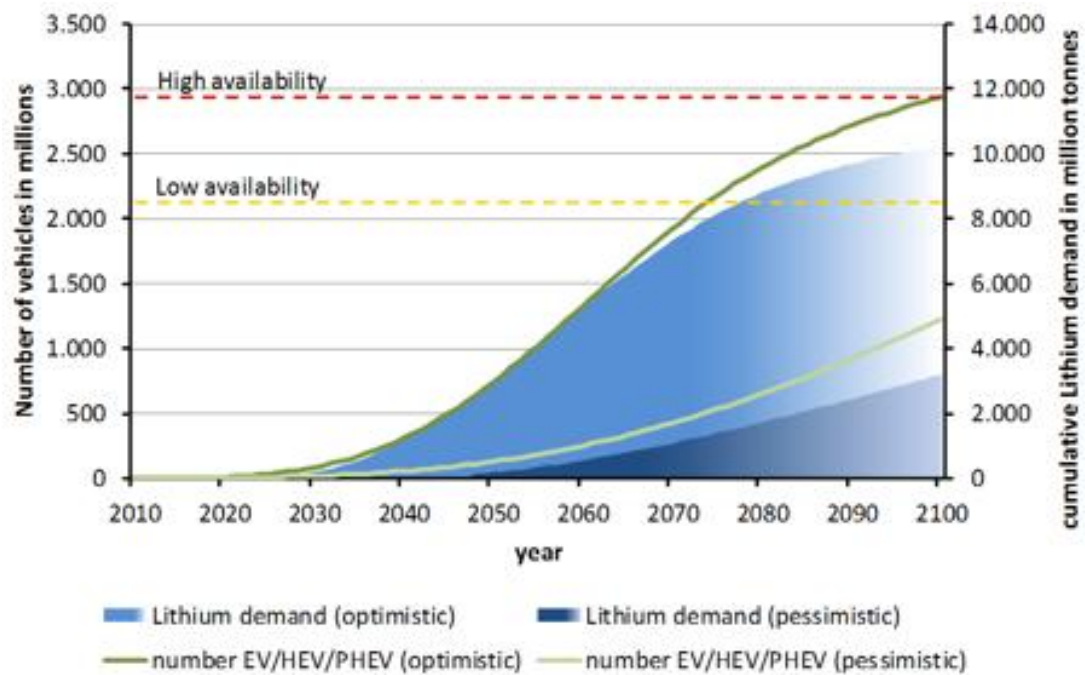
Figure 1-5. Scenario of Lithium consumption for future.[15]

1-2.Theoretical background

1-2-1. Electrolyte

Electrolyte which is component in NIBs .has been important issue to improve electrochemical performance. Electrolyte is composed of salt, solvent and additives. The performance of electrolyte highly depends on component and composition of it. Electrolyte has two major functions in NIBs which are Na^+ ion migration and making solid electrolyte interphase (SEI) on electrode.

Especially, Na^+ ion migration is highly related to ionic conductivity. Good ionic conductivity can make it easy to move Na^+ ion. As ionic conductivity is determined by viscosity and dielectric constant of solvent, it should be important issue to consider combination of sodium salt and solvent.

There are many kinds of sodium salt such as $NaPF_6$, $NaClO_4$ and $NaBF_4$. Each of salt has different chemical properties and electrochemical performance. In solvent, carbonate-based solvent is well known because it has great stability in SIBs.[20-21] The carbonate-based solvents are divided to cyclic and linear carbonate by molecular structure. The linear carbonate such as DEC, DMC and EMC has low viscosity and cyclic carbonate such as EC and PC dissociate sodium salt for migration.

1-2-2. Solid electrolyte interphase (SEI) layer

Making suitable SEI layer is key issue in SIBs. When batteries are charged or discharged, electrolyte which contact with electrode is decomposed on electrode surface. The decomposition material of electrolyte exists as interphase layer which inhibit to contact electrolyte with pristine electrode. However, Na^+ ion can pass through SEI layer to react with active materials. Nowadays, design of SEI layer is great attention to batteries research and highly related to electrochemical performance.

1-2-3. Functional additives

The electrolyte has great deal of attention as stable SEI layer directly connected to performance of batteries. Functional additives are introduced to supplement electrolyte for safety and stable SEI layer. When adding small amount of additives into electrolytes, additives can dynamically change the SEI layer's properties. In NIBs, the research of additives didn't have much studied. Therefore, the report of functional additives in LIBs can provide the model when we consider suitable additives to improve electrochemical performance. In case of anode, the effect of vinylene carbonate(VC),[22-23] fluoroethylene carbonate(FEC)[24-25] and succinic anhydride(SA)[26] are well studied as functional

additives to improve cycle performance. Especially, these additives change the surface chemistry of SEI layer in metallic anode and reduce surface resistance due to the formation of thin SEI layer.[27] In case of cathode, boron-based additive show enhancement of cycle performance due to suppress the oxidation reaction in high voltage.[28-29] Moreover, additives such as flame retardant which can reduce gas generation have key issue for battery safety. The phosphate-additive has been reported to increases thermal stability of electrolyte at the little effect of electrochemical performance.[30-31]

1-2-4. Molecular orbital (MO)

Molecular orbital builds on the electron wave functions of quantum mechanics to describe chemical bonding. There are highest occupied molecular orbital (HOMO) and lowest unoccupied molecular orbital (LUMO). HOMO is electron donating potential toward being able to accept electron and LUMO is electron accepting potential from being able to donate electron. When SEI layer is formed by oxidation of additives for cathode, the additives should be high HOMO energy. In the case of anode, the additives should be lower LUMO energy because additive should reduction reaction to make SEI layer on the anodes.

Chapter 2

Cyclic carbonate based-electrolytes enhancing electrochemical performance of $Na_4Fe_3(PO_4)_2(P_2O_7)$ cathode for sodium-ion batteries

2-1. Introduction

2-1-1. Research trend of cathode in NIBs

The needs for large-scale electric devices demand the low cost and safety batteries in recent years. Especially, Na-ion batteries seem to as a promising candidate for next-generation battery system because the natural abundance of Na resources and many similarities with Li-ion batteries. However, Na ion is larger ionic radius than Li ions as reversibility of Na insertion/extraction process.[18-19]

In Na-ion batteries, the cathode consists of sodium has reversibly insert/extraction process at a voltage greater than 2V. Especially, the energy density of the Na battery can be increased by increasing working voltage of cathode or decreasing it of anode. The Na^+ ion which increased size and mass compared to the Li^+ show slow diffusion in similar structure. Like a cathode of LIBs, sodium has various host materials like metal-oxide and poly-anion compounds. First, the layered $NaMO_2$ compounds have been introduced as Na-intercalation structure. For example, $NaCoO_2$ has P and O type structure.[32] Especially, P2-type $NaCoO_2$ can maintain their structure during Na insertion/extraction. This property of P2 type mean that it didn't need to Co-O bond cleavage. In addition, P2-type NaCoO2 show great cycle performance and high energy density (440wh/kg) when charged at 4.0V.[33] Recently, $NaNi_{0.5}Mn_{0.5}O_2$ which is solid solution compounds has been introduced for NIBs.[34] In LIB cases, $LiNi_{0.5}Mn_{0.5}O_2$ show poor rate performance due to the cation disorder between Li^+ and Ni^{2+}.[35] However, $NaNi_{0.5}Mn_{0.5}O_2$ didn't have cation disorder because Na^+ is much larger than Ni^{2+}. It shows about $125mAhg^{-1}$ specific capacity when charged at 3.8V and good rate performance.

Recently, $Na_4Fe_3(PO_4)_2(P_2O_7)$ which is mixed polyanion compound framework proposed as a promising cathode for Na rechargeable.[36] When the $Na_4Fe_3(PO_4)_2(P_2O_7)$ electrode has charged or discharged process, it occurs a one-phase reaction with a reversible Fe^{2+}/Fe^{3+} redox reaction and has small volumetric change of less than 4%. Therefore, small volume change is contributed to polyanion compounds which can rotate and distortive to relieve the structure change.[37] $Na_4Fe_3(PO_4)_2(P_2O_7)$ cathode show theoretical capacity of $129mAhg^{-1}$ and average voltage of 3.2V. Moreover it has good thermal stability up to 530 ℃ at all SOCs. The research of cathode will continue to increase capacity

and rate capability for NIBs.
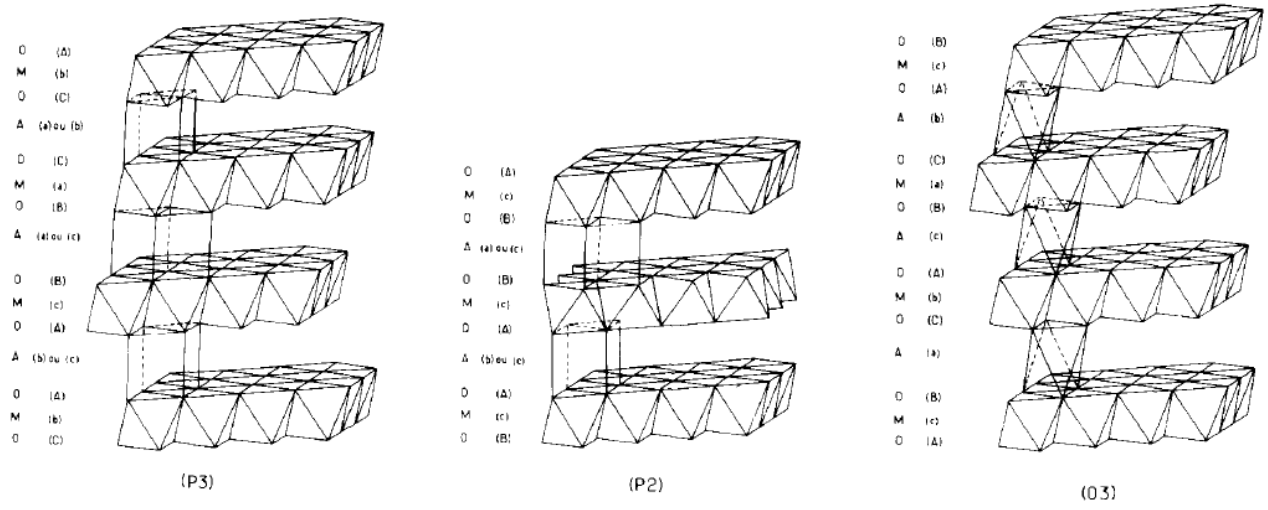
Figure 2-1. Various structure of $NaCoO_2$.[32]
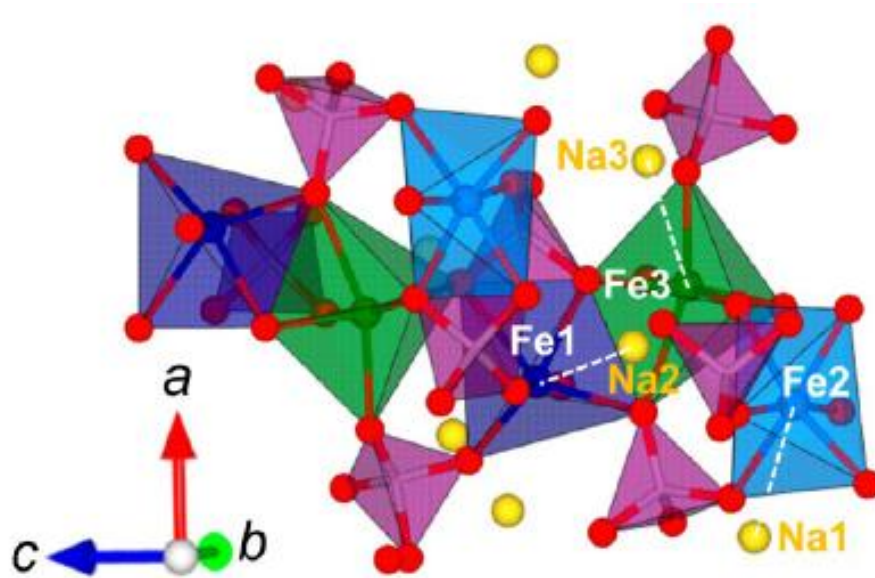
Figure 2-2. Local structure of $Na_4Fe_3(PO_4)_2(P_2O_7)$.[37]

2-1-2. The need of suitable electrolyte in $Na_4Fe_3(PO_4)_2(P_2O_7)$ cathode

,

In NIBs, there are many researches in architecture of electrode materials to improve performance. However, when the electrode materials accomplish their performance, interfacial reactions between electrolytes should be considered in batteries. In particularly, electrolytes are usually decomposed on electrode due to the high voltage. Therefore, reduing the decomposition of electrolyte and making a stable surface layer formed on the cathode determine the coulombic efficiency and long term cycle performance. Unfortunately, electrolyte field just show bulk properties and suitable candidate in NIBs.

In this work, we demonstrate key aspects of the electrolyte formulation to afford high electrochemical performances of $Na_4Fe_3(PO_4)_2(P_2O_7)$ cathode. The electrochemical performance of cathodes with different electrolytes Furthermore, we investigated the electrochemical reaction products on the cathode by means of ex-situ X-ray photoelectron spectroscopy (XPS) and the reactivity of the electrolytes toward Na metal electrode by ^{13}C NMR techniques.
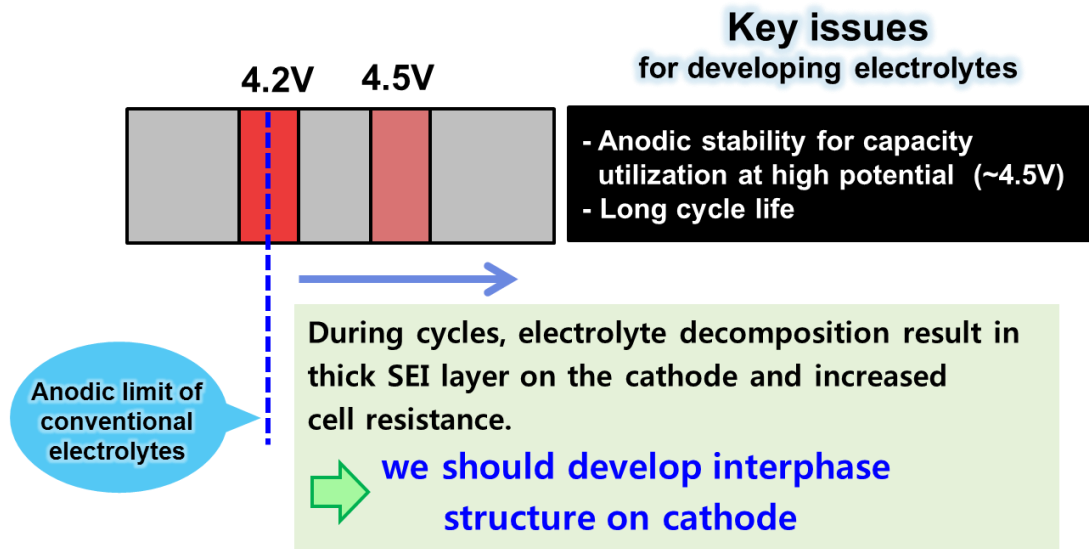
Figure 2-3. Key issue of electrolyte in cathode
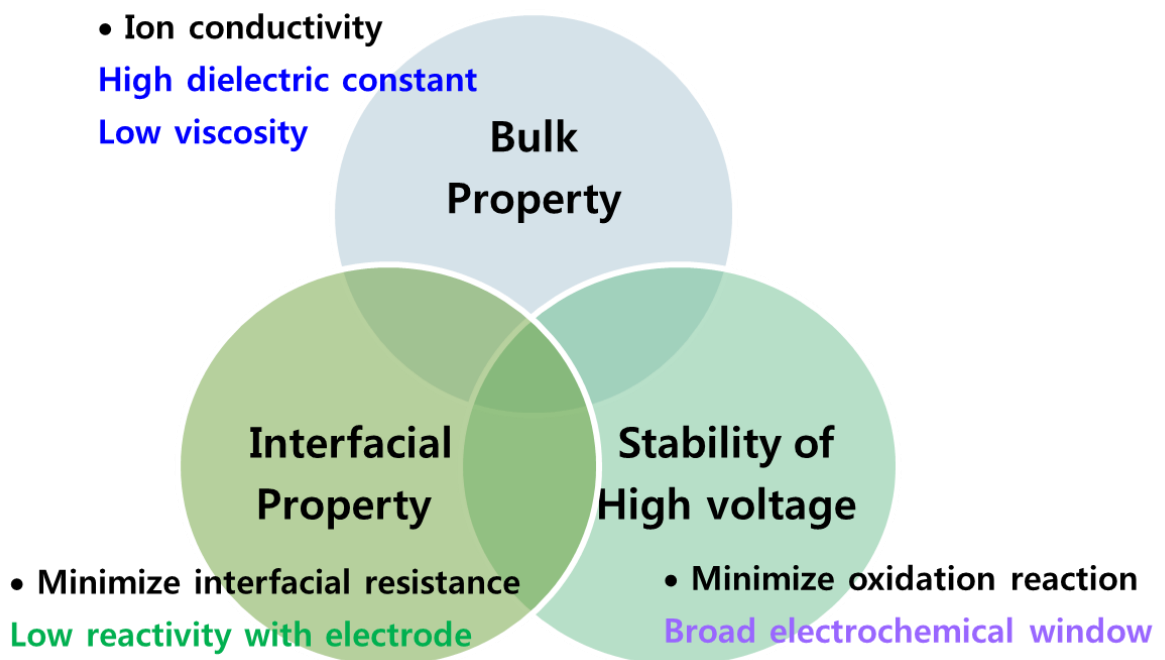
Figure 2-4. Demand of electrolyte for high performance in batteries

2-2. Experiment Section

2-2-1. Electrolyte characterizations

The electrolyte was composed of commercially available sodium perchlorate ($NaClO_4$) dissolved in each solvent mixture of ethylene carbonate (EC), diethylene carbonate (DEC) with a 5:5 volume ratio and propylene carbonate (PC) with 5:5 volume ratio. The attenuated total reflectance–Fourier transform infrared (ATR-FTIR) spectra of the electrolytes were recorded in reflectance measurements using a Varian 670-IR spectrometer with a spectral resolution of 4 cm^{-1} in a nitrogen atmosphere. The ionic conductivity of the electrolytes was measured using an Oakton CON 11 standard conductivity meter at room temperature.

2-2-2. Electrode preparation and electrochemical characterization

For the electrochemical tests, the electrode was prepared by spreading a slurry mixture of $Na_4Fe_3(PO_4)_2(P_2O_7)$, Polyvinylidene fluoride (PVDF binder) and super P (70:20:10 in weight ratio) on a Al foil. Galvanostatic cycling (WonATech WBCS 3000) was performed in a potential window of 4.2–1.7V with a 2032 coin-type half cell. Precycle and cycle performance of cells were performed at a rate of C/20 and C/10, respectively. The anodic limit of electrolyte solutions was determined by means of linear sweep voltammetry (LSV); we used stainless steel as the working electrode and sodium electrode as the reference and counter electrodes.

2-2-3. ^{13}C nuclear magnetic resonance (NMR) and surface analysis

^{13}C NMR spectra of electrolytes which contact with Na metal electrode were recorded on Agilenet (VNMRS 600) spectrometer. After 10days, each of electrolytes was carefully obtained in argon filled glove box and injected into NMR tube with THF-ds solvents. The surface morphology of the electrodes was observed with a field emission scanning electron microscope (FE-SEM; JEOL JSM-6700F). After precycle process, the cells were carefully opened in a glove box to retrieve their electrodes. The electrodes were then rinsed in dimethyl carbonate to remove the residual $NaClO_4$-based electrolyte, and the resulting materials were dried. Ex-situ X-ray photoelectron spectroscopy (XPS, Thermo Scientific K-Alpha system) measurements for dried cathodes were performed with Al Kα (hv = 1486.6 eV) radiation under ultrahigh vacuum. XPS spectra were taken using a 0.10 eV step and 80 eV pass energy. Samples were prepared in a glove box and sealed with an aluminum pouch film under a vacuum before use. Then, samples were rapidly transferred into a chamber of XPS instrument to minimize any possible contamination.

2-3. Results and discussions

2-3-1. The FT-IR spectra in electrolyte

Fig. 2-5 presents the FT-IR spectra of EC/DEC- and EC/PC-based electrolytes as a function of NaClO$_4$ concentration in the frequency regions, which are characteristic for the C–O and –CH$_2$– groups. A comparison of the FT-IR spectra for electrolytes with the increase of NaClO4 concentration reveals that clear differences exist, as shown in Figs. 2-5(a) and (b). The FT-IR spectra of Fig. 2-5(a) and (b) over a range from 870 to 930 cm^{-1} corresponding to the C-O single bond stretching of EC show that the proportion of solvated EC molecules interacting with L^{i+} ions at 902 cm^{-1} gradually increases with increasing NaClO$_4$ concentration. This result is persuasive evidence that EC effectively interacts with Na$^+$ ions. Figs. 2-5(c) and (d) show the FT-IR spectra of the region corresponding to the CH$_2$ wagging mode of EC solvent. A new peak at 1406 cm^{-1} was produced by introducing NaClO$_4$ to a solvent mixture of EC/DEC or EC/PC. The peak at 1406 cm^{-1} arises from the ion-dipole interaction between the CH$_2$ moieties of EC or PC and salt anions. The intensity of the CH$_2$ peak of EC interacting with ClO$_4^-$ anions in EC/PC-based electrolytes is comparatively weak compared to EC/DEC-based electrolytes, as presented in Figs. 2-5(c) and (d). This is because the coordination between CH$_2$-CH(CH$_3$) of PC in the EC/PC-based electrolyte and ClO$_4^-$ anions is possible.
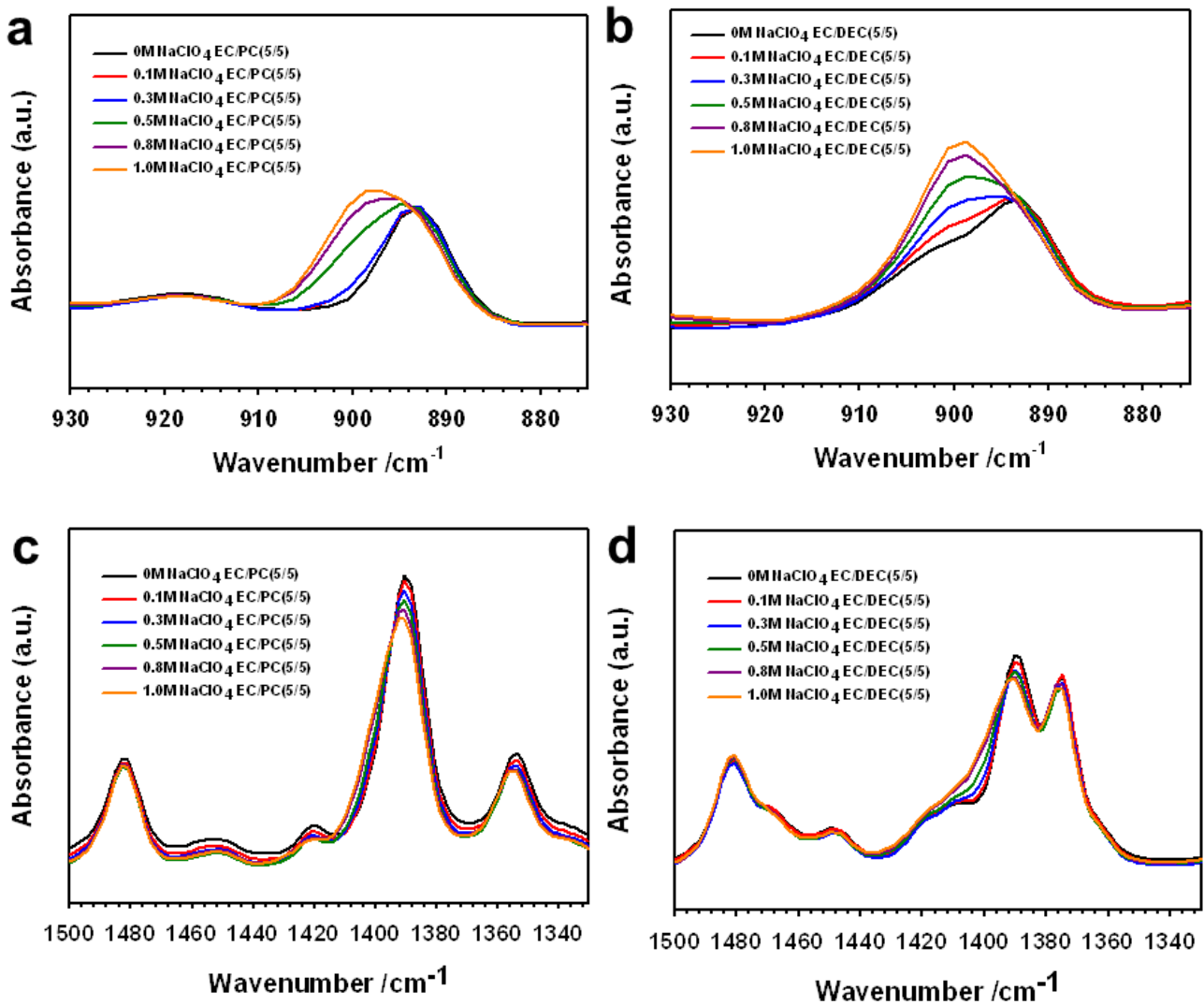
Figure 2-5. FT-IR spectra of various composition in $NaClO_4$ (a),(c) EC/DEC(5/5) and (b),(d) EC/PC(5/5).

2-3-2. The bulk properties of electrolyte

Fig. 2-6(a) exhibits the ionic conductivities of EC/DEC- and EC/PC-based electrolytes as a function of $NaClO_4$ salt at room temperature. Although the same concentration of $NaClO_4$ in a different solvent mixture was used, EC/PC-based electrolytes showed slightly higher ionic conductivities between 0.5 and 1.0 M $NaClO_4$. This implies that EC/PC solvent mixture is more effective than EC/DEC mixture to enhance ionic conductivities, which are governed by the charge carrier concentration and the mobility of charge carriers. The comparison of the oxidation stability of EC/DEC- and EC/PC-based electrolytes is shown in Fig. 2-6(b). The EC/DEC/1M $NaClO_4$ started to oxidize at 3.6V on a stainless steel electrode and showed appreciable oxidation currents over 4.0V vs. Na/Na^+. In comparison, EC/PC1M $NaClO_4$ did not show the significant oxidation currents up to 4.7V vs. Na/Na^+. This result suggests that EC/PC/1M $NaClO_4$ electrolyte is more stable at high voltage condition compared to EC/DEC/1M $NaClO_4$. This is in good agreement with the previous report, which the oxidation stability of the electrolyte is closely linked to solvent species.
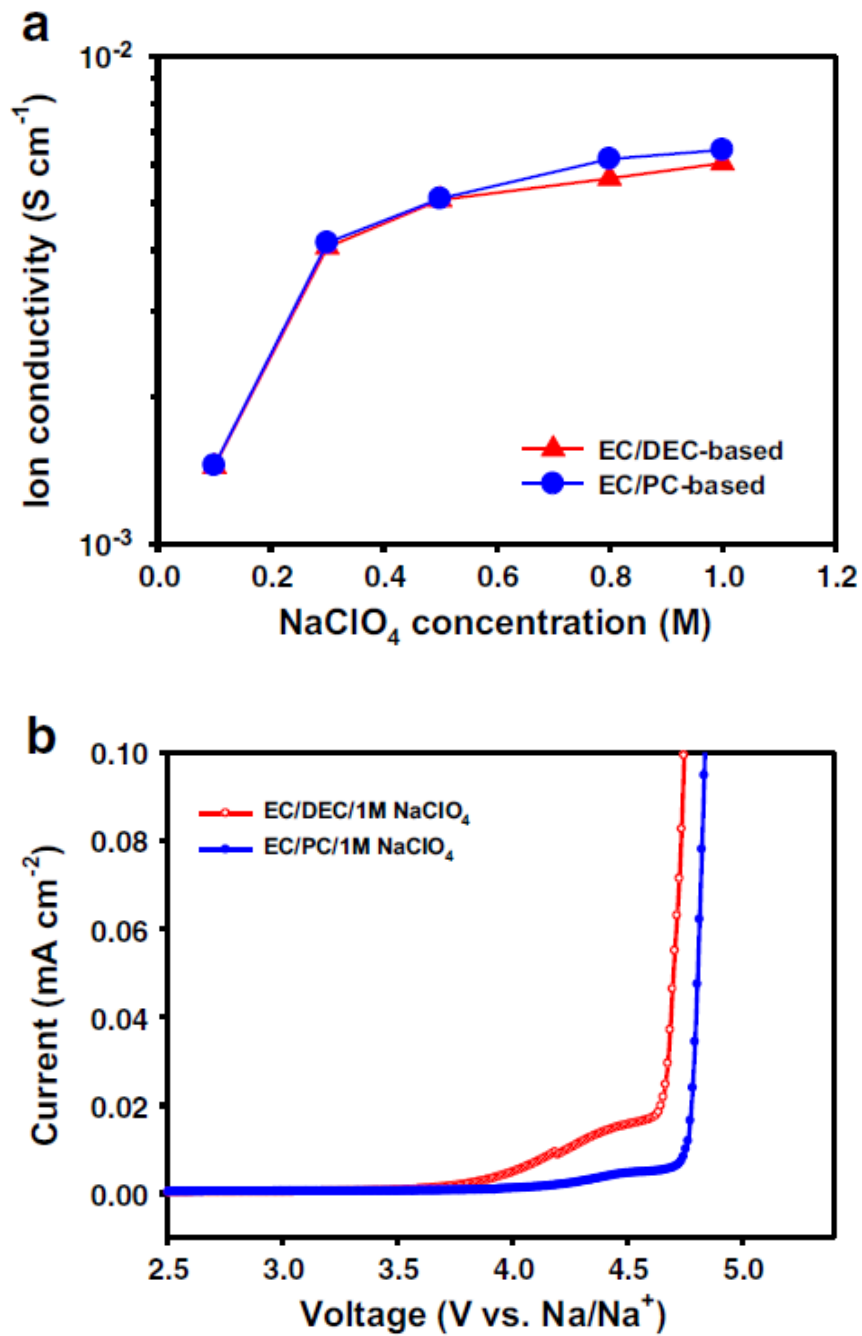
Figure 2-6. (a) Ionic conductivities of electrolytes with the $NaClO_4$ concentration at room temperature. (b) Linear sweep voltammetry of EC/DEC- and EC/PC-based electrolytes.

2-3-3. The electrochemical performance of $Na_4Fe_3(PO_4)_2(P_2O_7)$ cathodes

Figs. 2-7 (a) and (b) present the charge and discharge profiles of $Na_4Fe_3(PO_4)_2(P_2O_7)$ cathodes at precycle. A $Na_4Fe_3(PO_4)_2(P_2O_7)$/Na cell (the theoretical capacity of $Na_4Fe_3(PO_4)_2(P_2O_7)$ is 128.98 mAh g^{-1}) with EC/PC/1M $NaClO_4$ delivered higher discharge capacity of 128 mAh g^{-1} with the corresponding initial coulombic efficiency of 89.5% compared to EC/DEC/1M $NaClO_4$. The cathode with EC/DEC/1M $NaClO_4$ displays considerable overcharging with increased length of the voltage plateau at around 3.2 and 4.1V vs. Na/Na^+. The significant overcharging behavior of the cathode in EC/DEC/1M $NaClO_4$ led to drastically reduced initial coulombic efficiency of 41.8%. A photo of separators and Na metal electrodes retrieved from the $Na_4Fe_3(PO_4)_2(P_2O_7)$/Na half cells after precycle in EC/DEC/1M $NaClO_4$ and EC/PC/1M $NaClO_4$ is shown in the inset of Figs. 2-7(a) and (b) .

When the cell was cycled in EC/PC/1M $NaClO_4$, there was no significant color change in the separator and Na metal electrode. By contrast, the separator and Na metal electrode cycled in EC/DEC/1M $NaClO_4$ exhibited severe color change (inset of Fig. 2-7(b)). Moreover, the cathode with EC/DEC/1M $NaClO_4$ had two voltage plateau (A and B regions), which were not observed in EC/PC-based electrolyte (Fig. 2-7(b)). Voltage plateaus of A and B region may be ascribed to the decomposition of EC/DEC/1M $NaClO_4$ electrolyte at the Na electrode and the electrolyte decomposition of at the cathode, respectively.

The cathode in the cell with EC/PC/1MNaClO$_4$ delivered a relatively high reversible capacity of approximately 122 mAh g^{-1}; in addition, its discharge capacity remained nearly constant during 100 cycles and it exhibited a high coulombic efficiency of 99%. In contrast, the cathode with EC/DEC/1M $NaClO_4$ exhibited very low coulombic efficiency, indicating capacity loss during cycling and gradual capacity fading after 60 cycles. (Fig. 2-7 (c),(d))
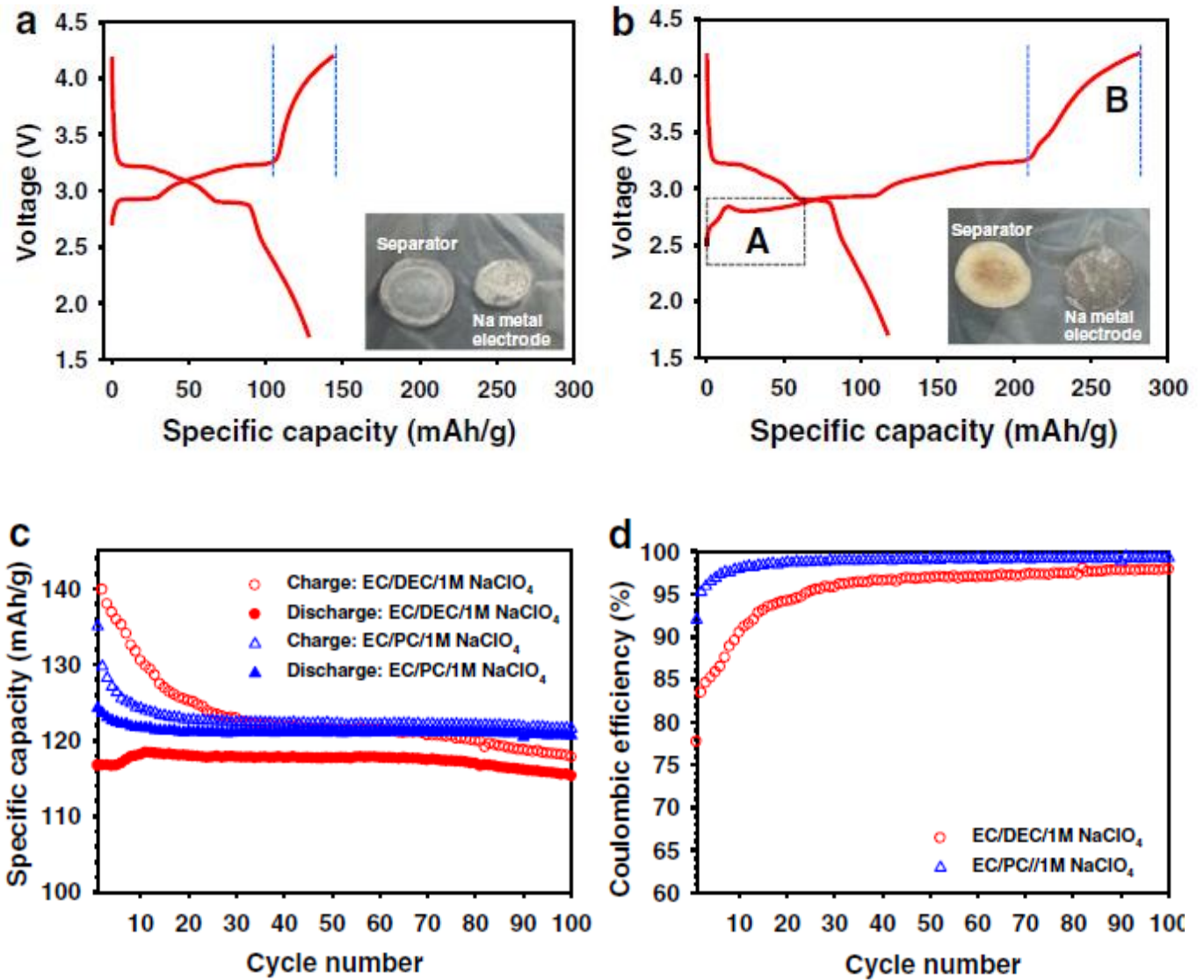
Figure 2-7. First voltage profiles of cathodes in (a) EC/PC-based or (b) EC/DEC-based electrolyte (C/20). (c) Cycling performance and (d) coulombic efficiency (C/10).

2-3-4. The electrolyte reaction with sodium metal

To investigate the reactivity of the electrolyte toward Na metal electrode, the composition of the electrolyte contacted with the Na metal electrode at room temperature for 10 days was investigated by ^{13}C NMR technique (Figs 2-8. (a) and (b)). After contacting with the Na metal for 10 days, new signals appeared at 65.2 and 66.8 ppm in EC/DEC/1M NaClO4.$NaClO_4$ contacted with the Na metal exhibited no new peaks, the peak at 66.8 ppm can be attributed to EC decomposed by reactive organic radical species ($CH_2CH_2\bullet$) resulting from DEC decomposition(Figs 2-9)

These results provide persuasive evidence that the EC and DEC solvents in EC/DEC/1 M $NaClO_4$ react with Na metal and that decomposition products (radicals, sodium alkyl carbonates) are formed in the electrolyte. These results also indicate that the EC/PC-based electrolyte is less reactive than EC/DEC toward the Na metal electrode (A region) and is relatively stable at high voltages (B region). It is thought that the resulting decomposition products diffuse to the cathode and accelerate the electrolyte decomposition at high potentials.
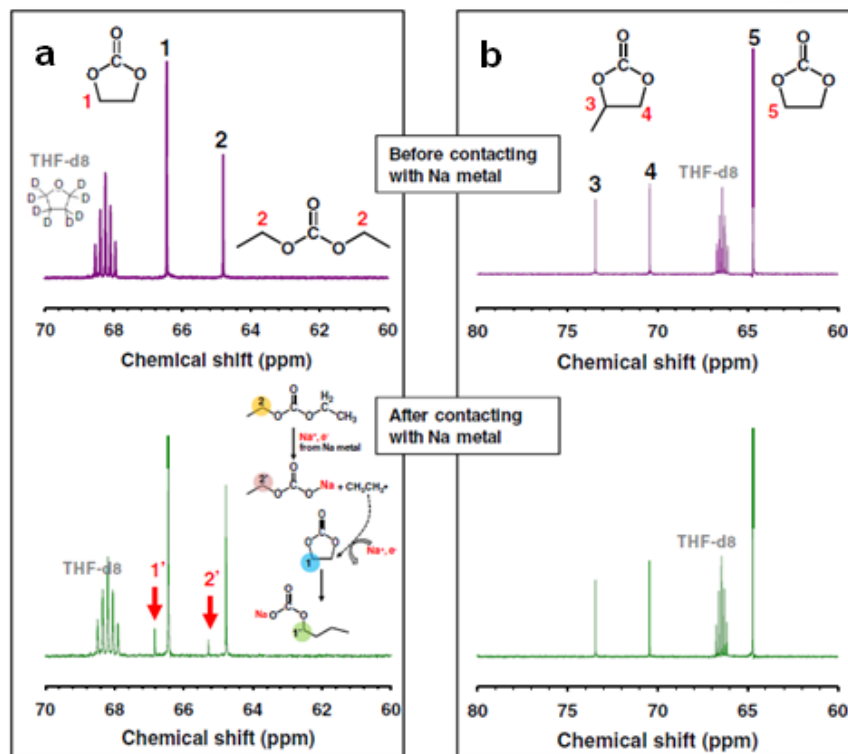
Figure 2-8. ^{13}C-NMRspectra of (a) EC/DEC/1MNaClO$_4$ and (b) EC/PC/1M NaClO$_4$ before and after contacting with Na metal for 10 days.
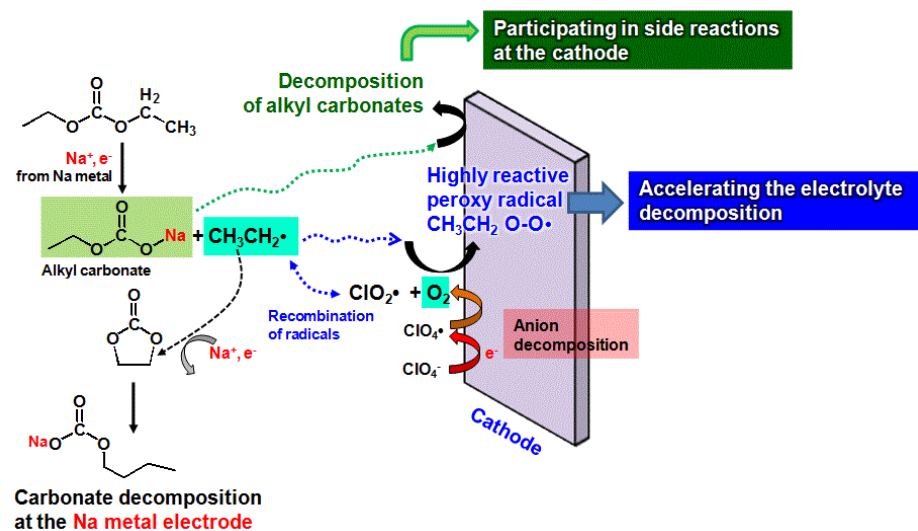
Figure 2-9. Schematic diagram of electrolyte decomposition on cathode

2-3-5. The surface morphology and component on the cathode

The surface morphology of $Na_4Fe_3(PO_4)_2(P_2O_7)$ cathode after precycle is shown in Fig. 2-10. The cathode cycled in EC/PC/1M $NaClO_4$ appears to be relatively clean and maintains homogeneous surface morphology. However, the cathode cycled in EC/DEC/1M $NaClO_4$ was covered by very thick SEI layer, which is produced by the oxidative decomposition of EC/DEC/1M $NaClO_4$ on the cathode during precycle.

To identify the decomposition products formed on the cathode, X-ray photoelectron spectroscopy (XPS) measurements were performed (Figs. 2-10 (d) and (e)). In the Cl 2p spectra, the peak at 200eV, which is assigned to Cl^-, was more intense in EC/DEC/1M NaClO4. In addition, the P 2p spectra shows that the peak corresponding to PO_4^{3-} and $P_2O7_4^-$ of $Na_4Fe_3(PO_4)_2(P_2O_7)$ discernibly disappears in EC/DEC/1M $NaClO_4$. This is because very thick SEI layer formed from the decomposition of EC/DEC/1M $NaClO_4$ blocks the P signal from the cathode. This result is consistent with the SEM observation that a thick SEI is formed on the cathode cycled in EC/DEC/1M $NaClO_4$.
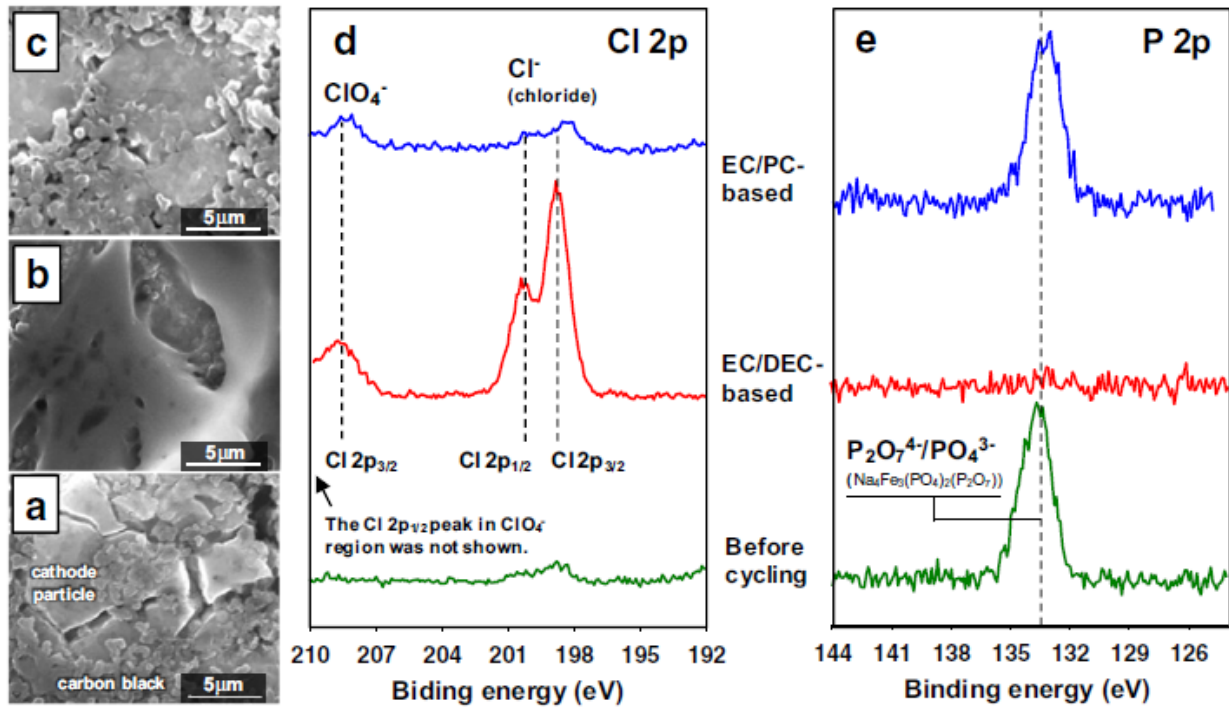
Figure 2-10. SEM images of (a) pristine $Na_4Fe_3(PO_4)_2(P_2O_7)$ cathode and cathodes cycled in (b) EC/DEC/1MNaClO$_4$ and (c) EC/PC/1MNaClO$_4$. (d) Cl 2p XPS spectra and (e) P 2p XPS spectra of cathodes before and after precycling.

2-4. Conclusion

In this research, I found that the use of EC/PC-based electrolyte is suitable in high voltage and sodium metal in NIBs. When $Na_4Fe_3(PO_4)_2(P_2O_7)$ cathode are charged up to 4.2V vs Na/Na^+, electrolyte decomposition are happened. Therefore, it is key issue to find stable electrolyte in high voltage. The EC/PC-based electrolyte not only endure electrochemical decomposition but also stable against the highly reactive Na metal. Moreover, I demonstrate surface chemistry on the cathode by using XPS and SEM analysis. I believed that these results can provide guidelines for advanced electrolytes with the promise of further improvement in electrochemical performances of Na-ion batteries.

Chapter 3

Interfacial architectures based on binary additive combination for high performance Sn_4P_3 anodes in sodium-ion batteries

3-1. Introduction

3-1-1. Research trend of anode in NIBs

In NIBs, Li-ion batteries seem to best model of electrode materials because Na-ion and Li-ion have many similarities. However, it is faced with difficulties to apply anode materials. In commercialized LIBs, graphite anode is layered structure and Li ion can intercalate this layer. In SIBs cases, sodium insertion to graphite layer is not favorable due to the large ionic size. To find alternative carbonaceous materials, hard carbon (HC) which is built by disordered graphene makes it possible that sodium ion electrochemically inserted into nanoporous of HC.[38-39] The initial capacity of hard carbon show $300 mAhg^{-1}$ which is closed to graphite in LIBs

Recently, alloy materials for SIBs have been introduced to overcome limitation of carbonaceous because it has high theoretical capacity such as Sn-based(about $994 mAhg^{-1}$),[40] P-based (about $2596 mAhg^{-1}$)[41-42] and Sb-based (about $660 mAhg^{-1}$).[43-45] Especially, Sn_4P_3 is promising anode materials for NIBs. The Sn_4P_3 anode materials exhibit high reversible capacity of $718\ mAhg^{-1}$ and reasonably low redox potential of about 0.3 V vs. Na/Na^+, which is beneficial for high operating voltage of a full cell.[46-48] Moreover, amorphous Na_3P matrix which is derived by conversion reaction during charge/discharge process can relieve pulverization of Sn particles. Further research of anode materials need to improve the cycle performance and rate capability
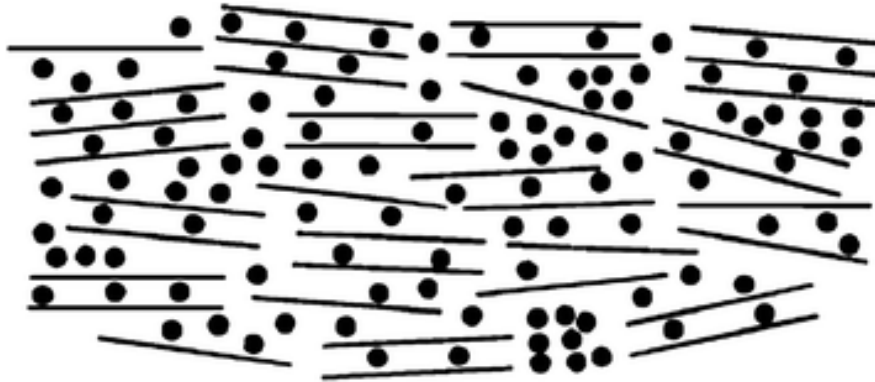
Figure 3-1. Structure of hard carbon filled by sodium or lithium.[38]
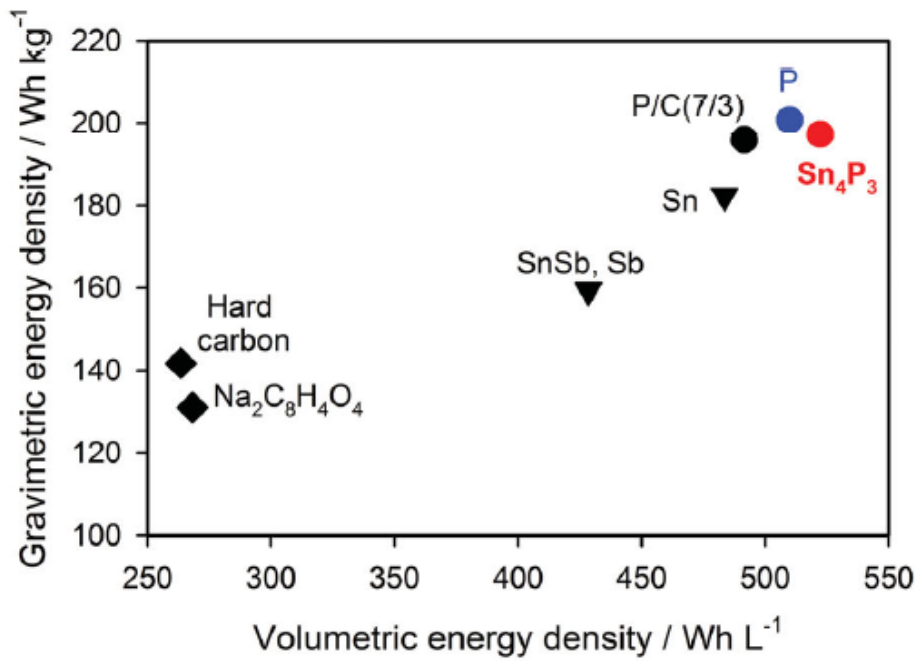
Figure 3-2. Gravimetric and volumetric energy density of anode in NIBs.[46]

3-1-2. The problem of Sn$_4$P$_3$ anode

Although Sn$_4$P$_3$ show high theoretical capacity and low redox potential, it has severe volume expansion during cycles. This volume expansion by Na insertion and extraction make cracking of the anode particles and lead to a continuous electrolyte decomposition on the exposed active surface of the anode.[46] The electrolyte decomposition directly makes thick solid electrolyte interphase (SEI)-filming and result in increasing interphase resistance.

To improve cycle performance, architecture of stable and robust protective layer on the metallic anode is critically important in NIBs. Significant SEI formation process depletes the limited Na$^+$ source in a cell, makes thick SEI layers provoking the loss of electrical conduction pathways in the electrode, and results in poor cycling performance. Therefore, it is already well known in LIBs that functional additives make stable SEI layer and greatly improve cycle performance. In case of NIBs, research cannot fully explain the function of additives and mechanism of SEI formations. To understand the interfacial characteristics and electrochemical reactions of the Sn$_4$P$_3$ anodes with and without additives, observations of surface morphology, spectral, and XRD studies of the Sn$_4$P$_3$ anode should be needed.
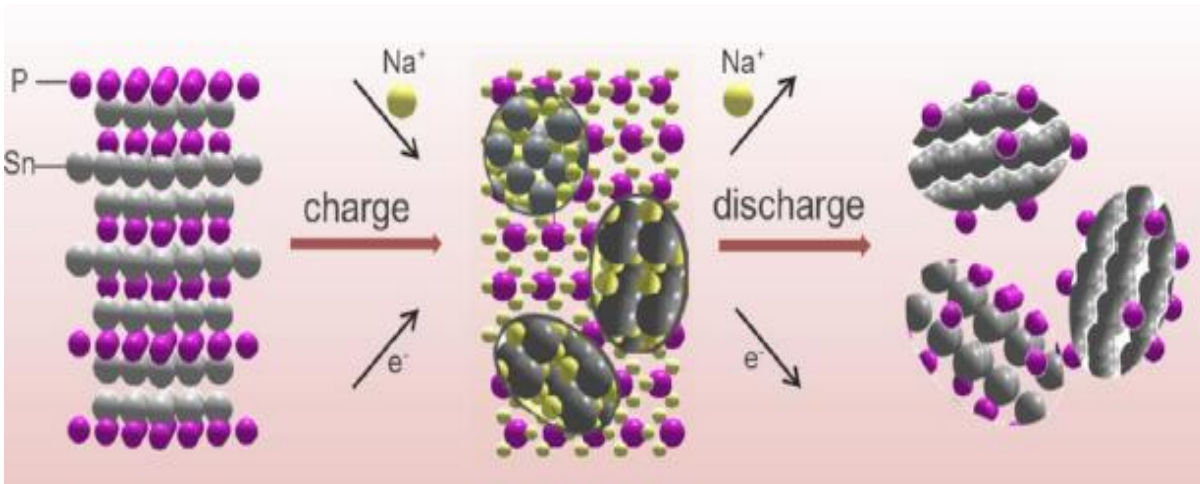
Figure 3-3. Structure of Sn_4P_3 particles during charge/discharge process.[48]
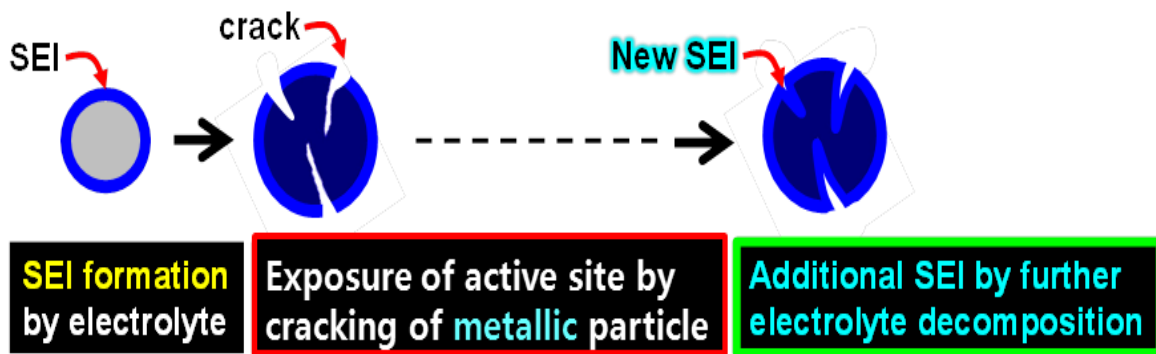
Figure 3-4. Formation of additional SEI layer during cycle

3-2. Experimental Section

3-2-1. Preparation electrolyte and electrode.

The reference electrolytes used for the electrochemical tests of Sn_4P_3/Na cells were 1 M sodium perchlorate ($NaClO_4$, Aldrich, $\geq$ 98.0%) dissolved in a solvent mixture of ethylene carbonate (EC)/propylene carbonate (PC) (1/1, v/v). Solvents (Soulbrain Co., Ltd.) were used as received. Fluoroethylene carbonate (FEC, Soulbrain Co. Ltd) and tris(trimethylsilyl) phosphite(TMSP, Aldrich) were introduced into the reference electrolyte as additives. For the electrochemical tests, the Sn_4P_3 anode material was synthesized according to a procedure reported in the literature. [46] The anode for the cell test was made of Sn_4P_3 active material, poly(acrylic acid) (PAA (M_w=100,000), Aldrich), and super P carbon black for electronic conductivity enhancement(70:20:10 in weight ratio) on a piece of Cu foil of 18 μm. The resulting anodes were dried in vacuum at 110 ℃ for at 2 hours prior to their assembly into cells.

3-2-2. Characterizations

After being precycled, the cells were carefully opened in a glove box to retrieve their anodes. The anodes were then rinsed in dimethyl carbonate to remove the residual $NaClO_4$-based electrolyte and were subsequently dried. The surface morphology of the anodes observed with a field-emission scanning electron microscope (FE-SEM; JEOL JSM-6700F). During characterization of the SEM image, an energy dispersive spectrometer (EDS) was also used to determine the kind of chemical components in the region under investigation. Ex-situ X-ray photoelectron spectroscopy (XPS, Thermo Scientific K-Alpha system) measurements were performed on the dried anodes using Al Kα (hν = 1486.6 eV) radiation under ultrahigh vacuum. XPS spectra were collected using a 0.10 eV step and an 80 eV pass energy. Samples were prepared in a glove box and sealed with an aluminum pouch film under vacuum before use. The samples were then rapidly transferred into the chamber of the XPS instrument to minimize any possible contamination. Anodes X-Ray diffraction (XRD) data were observed on a Rigaku D/MAX2500V/PC powder diffractometer using Cu-Kα radiation (λ = 1.5405 Å) operated in the 2θ range of 10-80. Cell impedances of 2032 coin-type half cells (Sn_4P_3 anode/metallic sodium) were monitored by means of an AC complex impedance analysis with an IVIUM frequency response analyzer over a frequency range of 10 mHz to 1 MHz.

3-2-3. Electrochemical measurements.

Galvanostatic charge and discharge cycling (WonATech WBCS 3000 battery measurement system) was performed with a two-electrode 2032 coin-type half cell at 30℃. Precycle and cycling tests of cells were performed in potential window from 0 V to 1.5 V vs. Na/Na$^+$ at rates of C/20 and C/10, respectively.

3-3.Result and Discussion

3-3-1. Electrochemical performance of Sn_4P_3 anodes with and without binary additive

Figure 3-5(a)-(c), show the voltage profiles of Sn_4P_3/Na half cells with and without functional additives (FEC and TMSP) for 1st, 5th, and 10th cycle at a rate of C/10 after precycle. The Sn_4P_3/Na half-cell with the baseline electrolyte delivered the Na extraction capacity of approximately $755 mAhg^{-1}$ in the 1st cycle and then its capacity was gradually decreased during the first 10 cycles, as presented in Figure 1a. After 30 cycles, severe capacity fading was observed for the Sn_4P_3 anode with the baseline electrolyte (Figure 3-5(d)). The Sn_4P_3 anodes with FEC- or FEC+TMSP-added electrolyte exhibited the Na extraction capacity of 600 $mAhg^{-1}$ and 605 $mAhg^{-1}$ at the 1st cycle, respectively and their capacity was maintained during the first 10 cycles (Figure 3-5(b),(c)). A comparison of Na extraction capacity of Sn_4P_3 anodes during 50 cycles clearly indicates that superior cycling stability is attained in the FEC+TMSP-added electrolyte, compared to the baseline and FEC-added electrolyte (Figure 3-5(d)). This result suggests that the formulation of FEC with TMSP additive leads to good electrochemical reversibility of the Sn_4P_3 anode.

Figure 3-6 shows the voltage profiles of Sn_4P_3 anodes at precycle. It is clear that the baseline electrolyte delivers relatively high Na insertion capacity of 1131 $mAhg^{-1}$, compared with the FEC-added (720 $mAhg^{-1}$) or FEC+TMSP-added (852 $mAhg^{-1}$) electrolyte. This relatively high Na insertion capacity of Sn_4P_3 anode with the baseline electrolyte may be attributed the voltage plateau at around 0 V vs. Na/Na^+, which is also observed for the first 10 cycles of Figure 3-5(a)-(c).
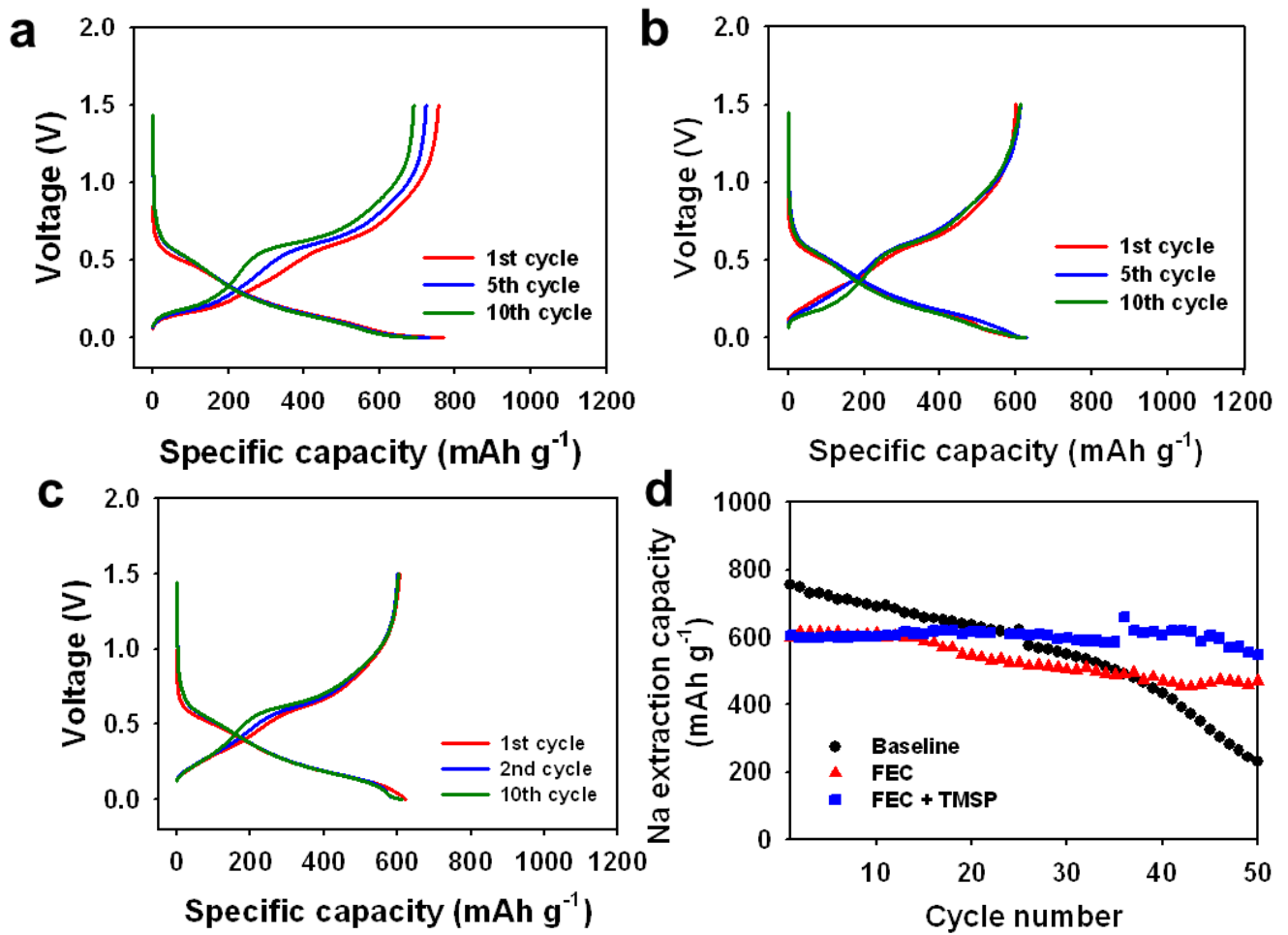
Figure 3-5. Voltage profiles of the Sn_4P_3 anodes cycled in (a) baseline, (b) FEC-added, and (c) FEC+TMSP-added. (d) Na extraction capacity of the Sn_4P_3 anodes at a rate of C/10.
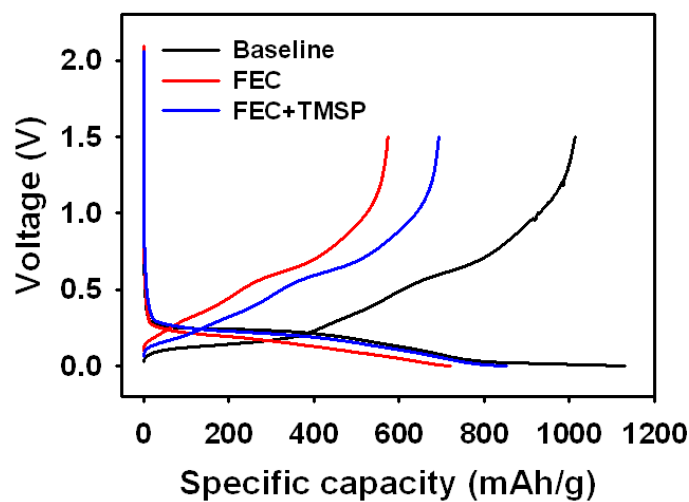
Figure 3-6. Voltage profiles of the Sn_4P_3 anodes during precycle at a rate of C/10.

3-3-2. dQ/dV plot and mechanism of Sn_4P_3 anodes with and without binary additive

The appearance of voltage plateau at around 0 V (B peak) in the baseline electrolyte is more clearly depicted in the dQ/dV graph of Figure 3-7(a),(d). The Sn_4P_3 anode with FEC-added electrolyte showed no B peak at around 0 V during a Na insertion at precycle (Figure 3-7(b)). Considerably reduced B peak appeared for the FEC+TMSP-added electrolyte (Figure 3-7(c)). To understand the difference of the dQ/dV graphs for the Sn_4P_3 anodes with and without additives, the origin of five main peaks (A to E) at precycle is needed to be discussed. During a sodiation process (Na insertion), the Sn_4P_3 anode can form three Na-Sn binary alloys corresponding to NaSn, Na_9Sn_4 and $Na_{15}Sn_4$ phase.[49]

At around 0.2 V corresponding to A peak during a sodiation process, the Sn_4P_3 is converted to NaSn, Na_9Sn_4 and Na_3P alloy materials ($Sn_4P_3 \rightarrow NaSn + Na_9Sn_4 + Na_3P$). At around 0 V (B peak) during a sodiation process, Na-Sn-based alloy materials are converted to Na_4Sn_{15} phase, which leads to severe volume expansion of the anode ($NaSn + Na_9Sn_4 + Na_3P \rightarrow Na_{15}Sn_4$). [40] At around 0.15 V (C peak) during a desodiation process (Na extraction), $Na_{15}Sn_4$ electrochemically oxides to form NaSn, Na_9Sn_4 and Na_3P phase ($Na_{15}Sn_4 \rightarrow NaSn + Na_9Sn_4 + Na_3P$). Two peaks at 0.3 V and 0.65 V during a desodiation process reflect the desodiation of NaSn, Na_9Sn_4 and Na_3P phase. As described previously, the B peak is closely linked to the formation of $Na_{15}Sn_4$ showing huge volume expansion.
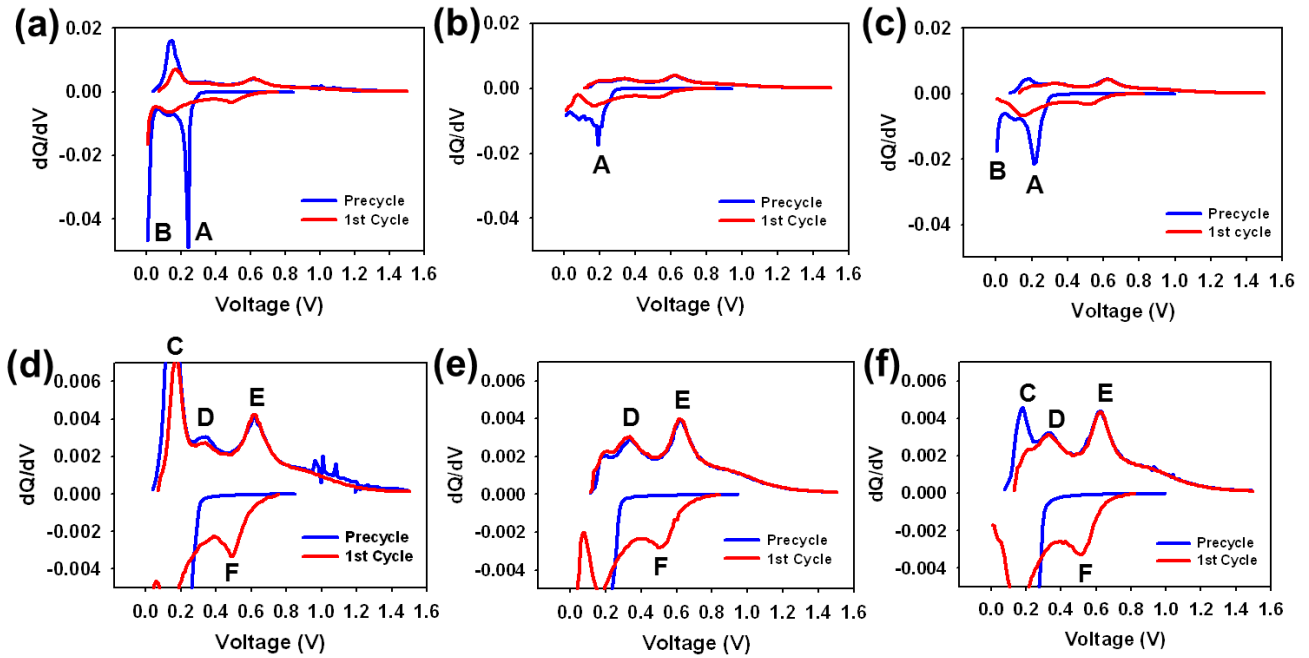
Figure 3-7. Differential capacity plots (dQ/dV) of precyle and 1st cycle in (a,d) baseline, (b,e) FEC-added, and (c,f) FEC+TMSP-added electrolyte.

3-3-3. The XRD pattern of Sn_4P_3 anodes

To further confirm the origin of the B peak observed in the baseline electrolyte, ex situ XRD patterns of the Sn_4P_3 anodes before and after precycle were obtained, as shown in Figure 3-8. Before precycle, the peaks corresponding to the crystalline phase of Sn_4P_3 are clearly shown in Figure 3-8(b). At a fully sodiated state, the broad peak corresponding to $Na_{15}Sn_4$ at $34°$ appeared for the Sn_4P_3 anode with the baseline electrolyte.[46] On the other hand, this broad peak was not observed for the FEC- and FEC+TMSP-added electrolyte (Figure 3-8(a)). This means that the $Na_{15}Sn_4$ phase is readily produced in the baseline electrolyte, compared to the FEC- and FEC+TMSP-added electrolyte. After full desodiation, the broad peak corresponding to $Na_{15}Sn_4$ phase mostly disappeared (Figure 3-8(b)). Importantly, the crystalline phase of anode materials was not generated even after a full desodiation.

This is because the crystalline structure of the Sn_4P_3, which was destroyed by a sodiation, was not recovered after a full desodiation process. From the XRD studies, it is thought that the B peak at around 0 V, which appeared for the baseline electrolyte, is greatly related to the formation of $Na_{15}Sn_4$ phase during a sodiation process. Interestingly, the presence of FEC in the electrolyte led to the formation of Na_9Sn_4 rather than $Na_{15}Sn_4$, as presented in the XRD pattern of Figure 3-8(a). This implies that the formation of $Na_{15}Sn_4$ phase can be inhibited by the FEC additive. Since this $Na_{15}Sn_4$ phase produced via further sodiation makes further capacity, the Sn_4P_3 anode with the baseline electrolyte could deliver slightly high Na insertion capacity. (Figure 3-5(a),(d) and Figure 3-6)

Figure 3-8. Ex-situ XRD pattern of Sn_4P_3 anodes (a) after full sodiation process and (b) after full desodiation process in the baseline, FEC-added, and FEC+TMSP-added electrolyte.

3-3-3. SEM and EDS analysis of Sn_4P_3 anodes after precycle

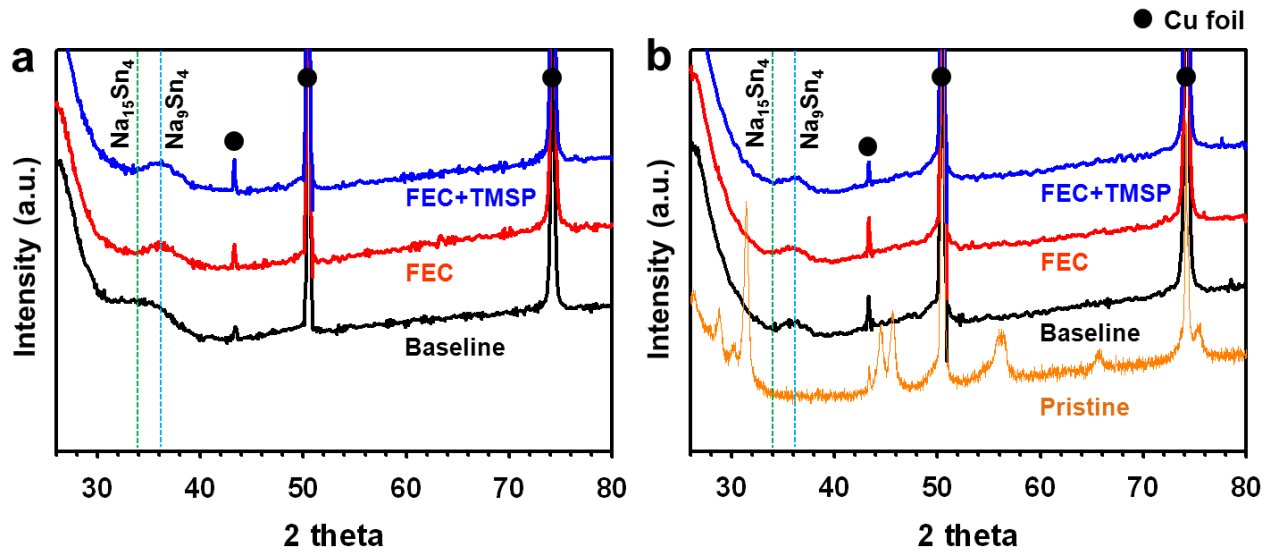Severe volume expansion via the formation of $Na_{15}Sn_4$ phase during a sodiation (Na insertion) process can result into agglomeration, cracking or pulverization of anode particles. Indeed, the aggregation of anode particles between 1 and 2µm occurred after precycle in the baseline electrolyte, as presented in Figure 3-9(a),(b). The size of aggregated anode particles was over 3 µm (Figure 3-9(b)). On the contrary, significant agglomeration of anode particles was not observed for the anode precycled in the FEC- and FEC+TMSP-added electrolyte (Figure 3-9(c),(d)). Especially, the anode precycled in the FEC+TMSP-containing electrolyte maintained the original morphology of anode particles very well. This result suggests that good electrical connection in the anode with the FEC+TMSP binary additive is preserved during cycling. Superior cycling stability of the anode with the FEC+TMSP-added electrolyte can be explained by this maintained anode morphology.

Moreover, the formation of $Na_{15}Sn_4$ phase in the anode is not desirable because considerable volume changes cause continuous electrolyte decomposition on the newly exposed metallic anode surface by the cracking and thereby thick solid electrolyte interphase (SEI) layers, which can impede the migration of Na ions into the anode, are produced on the anode surface. To identify the decomposition products formed on the Sn_4P_3 anode, an energy dispersive spectrometer (EDS) measurements were performed during characterization of the SEM image (Figure 3-9(e),(f)). Zone A selected from the anode precycled in the baseline electrolyte displays the pronounced carbon (C), oxygen (O), and chlorine (Cl) signals, which are produced by the unwanted decomposition of EC/PC solvents and ClO_4^- anion. These C, O, and Cl signals were detected on not the Sn_4P_3 anode particles but carbon black particles, as shown in Figure 3-9(b). This result indicated that the electrolyte decomposition takes place on carbon black particles and thereby the decomposition byproducts protect the anode surface. For zone B selected from the anode with the FEC-containing electrolyte, a strong fluorine (F) signal formed by the FEC decomposition and relatively reduced C, O, and Cl signals appeared (Figure 3-9(f)). This indicates that the FEC electrochemically reduces on the anode prior to the electrolyte decomposition and effectively suppresses the decomposition of solvents and salt.
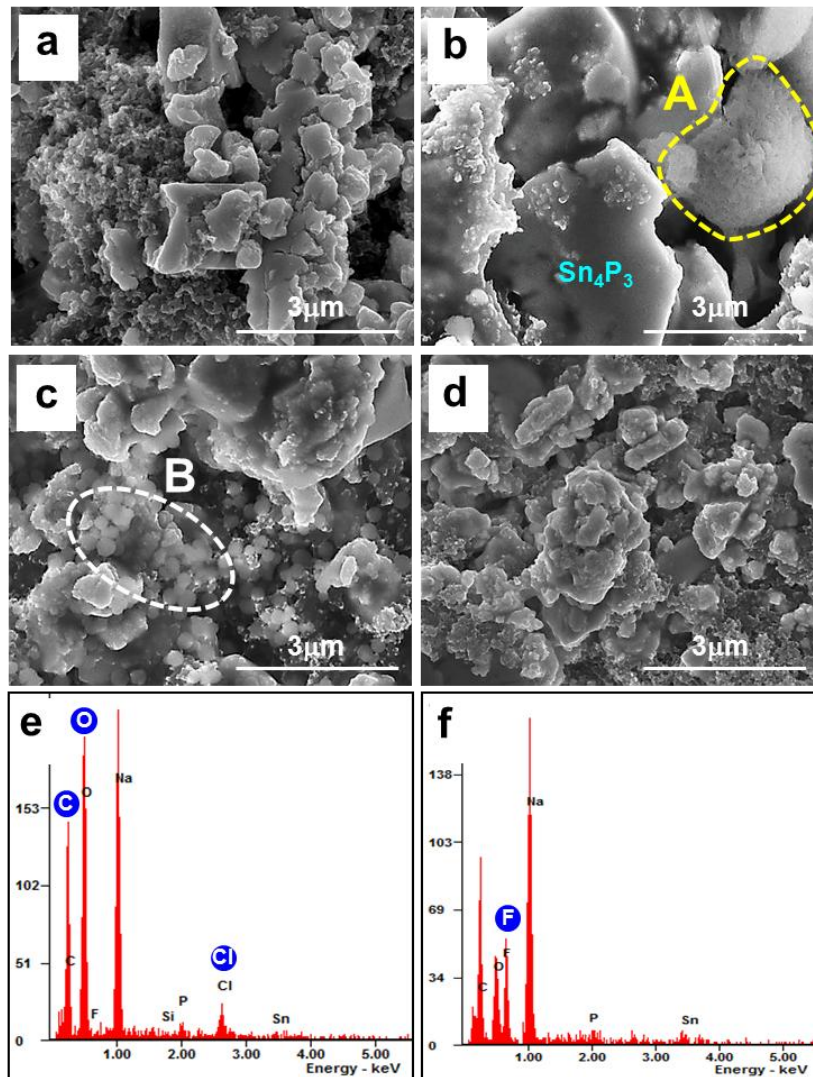
Figure 3-9. The SEM images of (a) pristine Sn4P3 anodes and after precycle in (b) baseline, (c) FEC-added, (d) FEC+TMSP-added electrolyte. The EDS spectra of Sn_4P_3 in (e) baseline and (f) FEC-added electrolyte.

3-3-4. XPS analysis of Sn_4P_3 anode after precycle

To clarify the origin of this peak in the dQ/dV graphs of Figure 3-7(d)-(f), ex-situ X-ray photoelectron spectroscopy (XPS) measurements were carried out. The Sn 3d XPS spectra of Figure 3-10 clearly showed that for all electrolytes, the peak assigned to the Sn metal, which can be formed via $NaSn + Na_9Sn_4 + Na_3P \rightarrow Sn + P + Sn_4P_3$,[48] appears at around 485 eV[50] after precycle. This resulting Sn metal, which was absent in pristine anode, undergoes the electrochemical sodiation at the subsequent cycle and thus the F peak at around 0.5 V is expected to correspond to the solidation of Sn metal.[40][47] Previously, the Yang group mentioned that Sn nanocrystals with low crystallinity are generated in the amorphous host matrix after Na insertion/extraction process. It is rationale that no peaks corresponding to the Sn metal were observed in the XRD pattern of the anode after precycle, possibly because the nanocrystallized Sn metal was formed for our anode system.[48] It was reported the resulting P formed by the Na extraction from Na_3P alloy can react with Na at the subsequent Na insertion process. The P 2p XPS spectra of Figure 3-11 clearly shows the existence of the P-O groups (134 eV) rather than the elemental P (~130 eV)[51] in the Sn_4P_3 anode after precycle. The P-O groups may be formed by the reaction of P with unstable byproducts formed by the solvent decomposition. From the Sn 3d and P 2p XPS results, it can be thought that the F peak in the dQ/dV graphs of Figure 3-7(d)-(f) closely linked to the sodiation of Sn metal during a Na insertion process.

Figure 3-10. Sn 3d XPS spectra of (a) pristine Sn_4P_3 anodes and after precycle in (b) baseline, (c) FEC-added and (d) FEC+TMSP-added electrolyte..
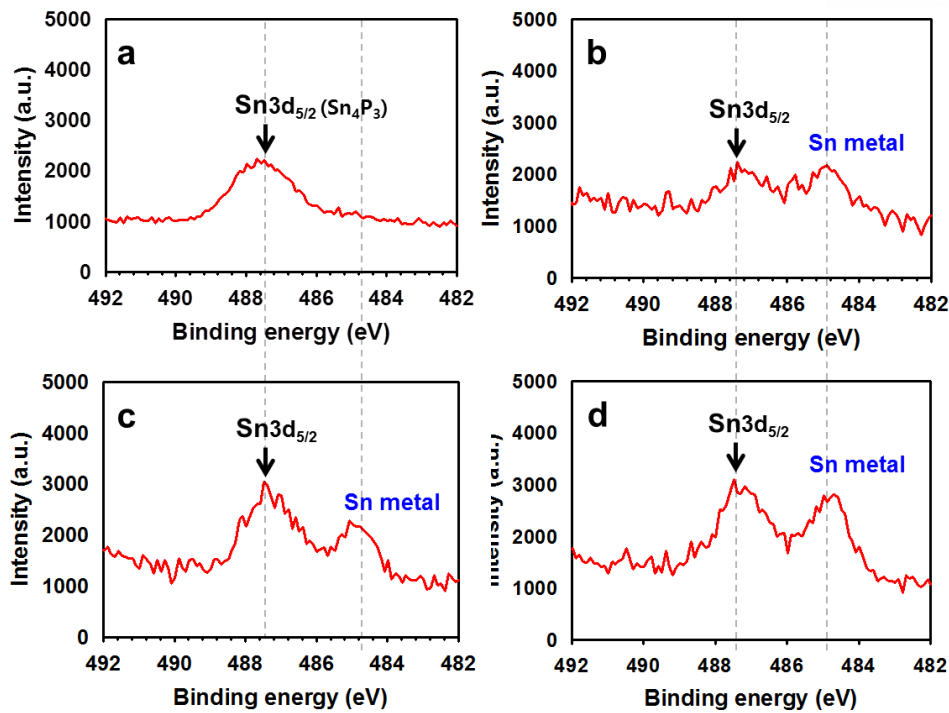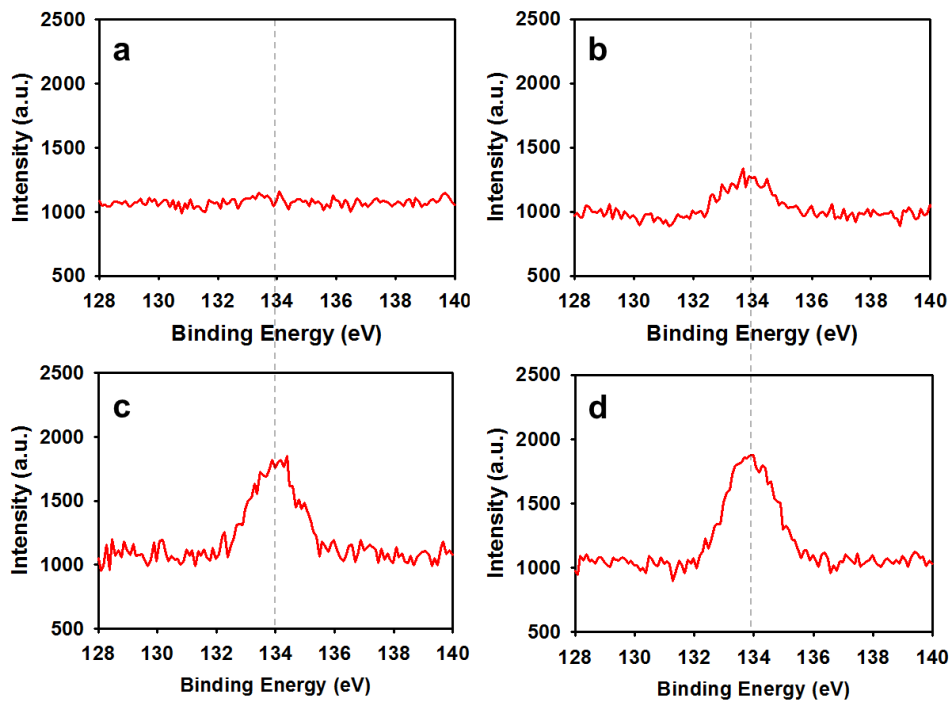

Figure 3-11. P 2p XPS spectra of (a) pristine Sn_4P_3 anodes and after precycle in (b) baseline, (c) FEC-added and (d) FEC+TMSP-added electrolyte

The F 1s spectra of Figure 3-12(g) and (h) show that the peak assigned to NaF at around 685 eV is observed for the FEC- and FEC+TMSP-added electrolyte. NaF is believed to be formed by the FEC decomposition on the anode.[52] Interestingly, the NaF peak intensity was drastically decreased for the FEC+TMSP-containing electrolyte. This result suggests that TMSP additive suppresses the formation of large amount of NaF by the FEC decomposition on the Sn_4P_3 anode. The unique function of TMSP for eliminating HF from FEC additive is proposed in Figure 3-12(a).

This HF removal can reduce the NaF formation in the SEI on the Sn_4P_3 anode. In addition, the Si-F moiety may be formed via the reaction of TMSP with HF from FEC, as depicted in Figure 6a. Moreover, byproducts formed by TMSP decomposition may contribute to the components of the SEI layer. Evidence for the presence of Si-F and Si-O groups in the SEI layer on the anode precycled in the FEC+TMSP-added electrolyte is given in the Si 2p spectra of Figure 3-12(d).

As clearly shown in Figure 3-7(a),(b) and 3-8(a), unlike the baseline electrolyte, the FEC-added electrolyte inhibited the formation of $Na_{15}Sn_4$ phase. This behavior can be explained by the NaF-based SEI generated via the FEC decomposition, as illustrated in Figure 3-13. The NaF resistive layer is thought to impede the migration of Na ions into the anode and thus the formation of $Na_{15}Sn_4$ phase causing huge volume expansion of Sn_4P_3 anodes is effectively prevented.

Figure 3-12. Si 2p and F 1s XPS spectra of (a,e) pristine Sn_4P_3 anodes and after precycle in (b,f) baseline, (c,g) FEC-added and (d,h) FEC+TMSP-added electrolyte.
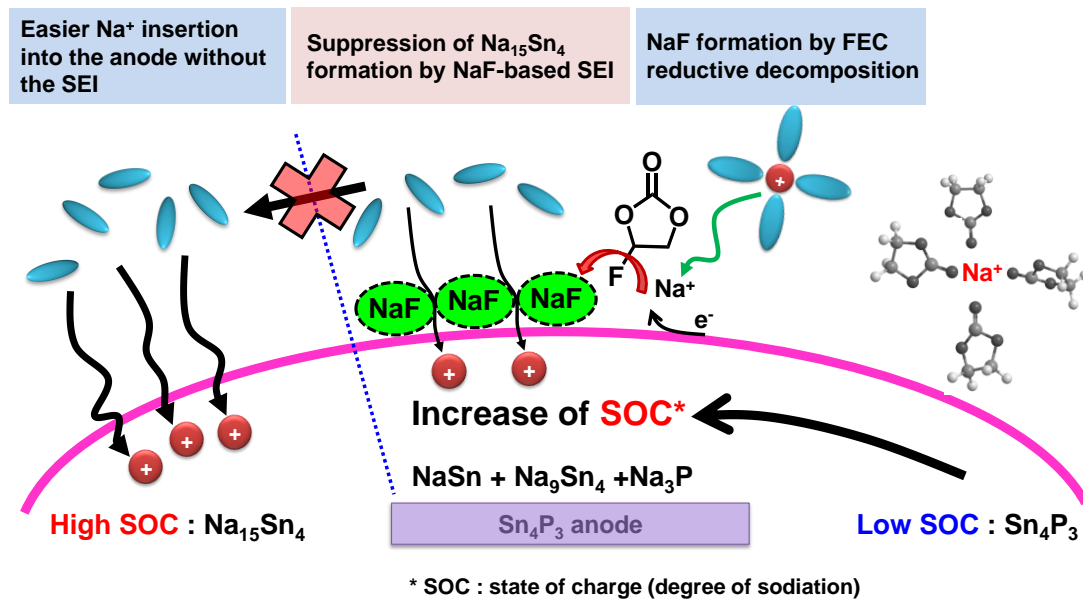

Figure 3-13. Schematic illustration showing the function of NaF-based SEI layer during sodiation process.

The C 1s XPS spectra of Figure 3-14(b) clearly exhibit that the peaks assigned to ether (C-O-C) moiety and sodium carbonate (Na_2CO_3) are more intense for the Sn_4P_3 anodes cycled in the baseline electrolyte, compared to the FEC- and FEC+TMSP-containing electrolyte. The ether and Na_2CO_3 can be generated by the EC decomposition (Figure 3-15). This result is in good agreement with the EDS results that strong C, O, and Cl signals formed by the electrolyte decomposition are detected on the anode precycled in the baseline electrolyte. It is obvious that the FEC and TMSP additives effectively prohibit the formation of ether and Na_2CO_3 by the EC decomposition, as presented in Figure 3-14(c),(d). In addition, the comparison of the C 1s XPS spectra of Figure 3-14(b)-(d) indicates that the peak corresponding to the C-C of carbon black particles discernibly decreases in the case of baseline electrolyte. This diminishment in the C-C peak intensity is attributed to a very thick surface film formed from the decomposition of the baseline electrolyte blocking the C-C signal from carbon black particles. This result is consistent with the SEM observation showing the formation of the SEI layer on the carbon black (zone A of Figure 3-9(b)).
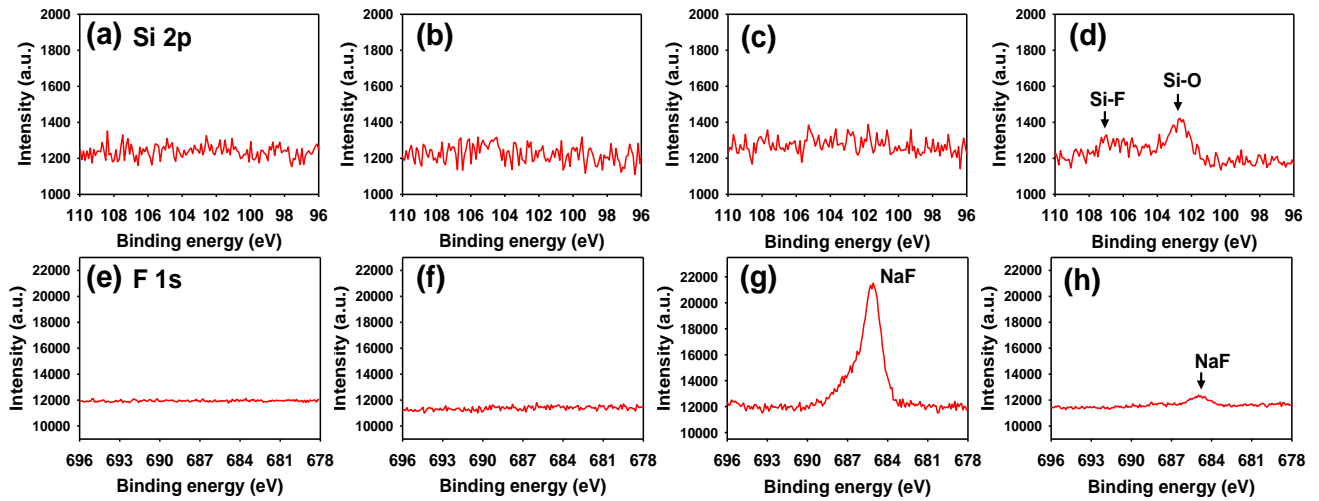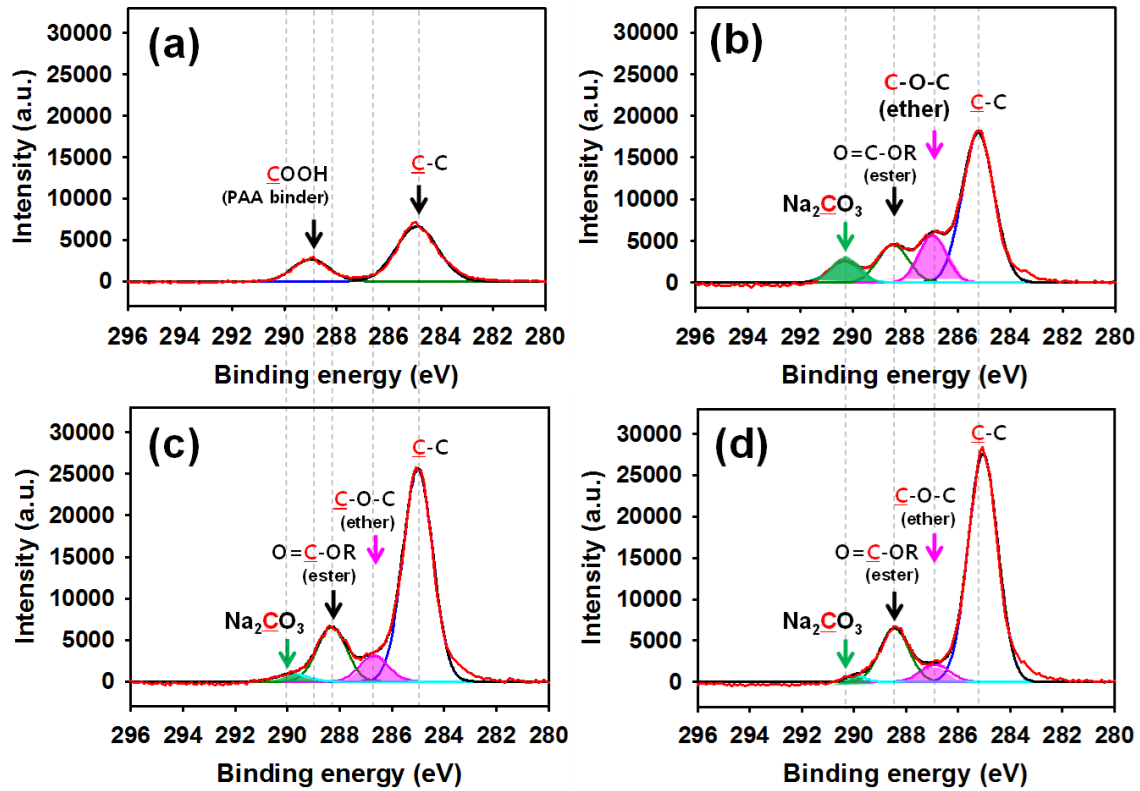
Figure 3-14. C 1s XPS spectra of (a) pristine Sn_4P_3 anodes and after precycle in (b) baseline, (c) FEC-added and (d) FEC+TMSP-added electrolyte.
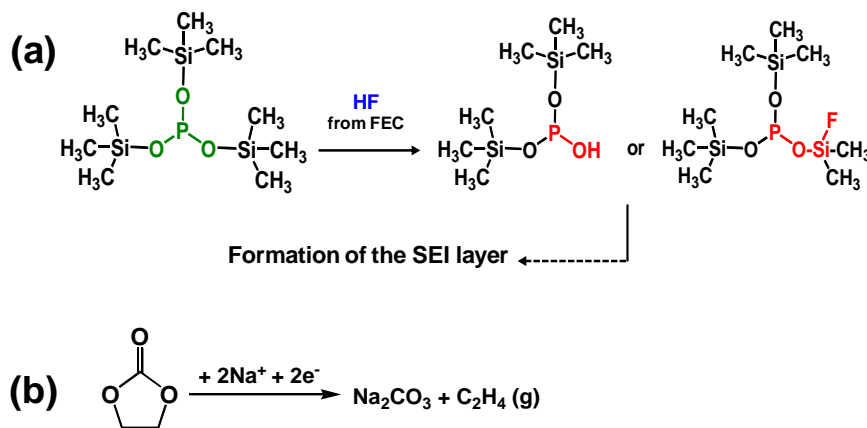
**Figure 3-15.** Schematic representation of possible mechanisms for (a) unique function of TMSP scavenging HF from the FEC and contributing the SEI formation on the anode, and (b) electrochemical reaction of EC with Na ions and electrons

3-3-5. AC impedance spectra of Sn$_4$P$_3$ anodes after full sodiation

Figure 3-16 shows AC impedance spectra of Sn$_4$P$_3$ anodes before and after full sodiation. A remarkable feature is that the interfacial resistance including the SEI resistance and charge transfer resistance components is higher for the Sn$_4$P$_3$ anodes of full sodiation in the FEC- and FEC+TMSP-added electrolyte, compared with the baseline electrolyte. This finding suggested that the NaF produced by the FEC decomposition acts as a highly resistive layer for the formation of Na$_{15}$Sn$_4$ phase showing severe volume expansion. The semicircle of the Sn$_4$P$_3$/Na half cells with FEC+TMSP after full sodiation was slightly smaller than that of the anode with the FEC-added electrolyte, possibly because the TMSP additive modified the NaF-based SEI layer. The hybrid SEI layer formed by the decomposition of binary additive (FEC+TMSP) also showed high interfacial resistance and thereby the formation of Na$_{15}$Sn$_4$ phase could be avoided during cycling.
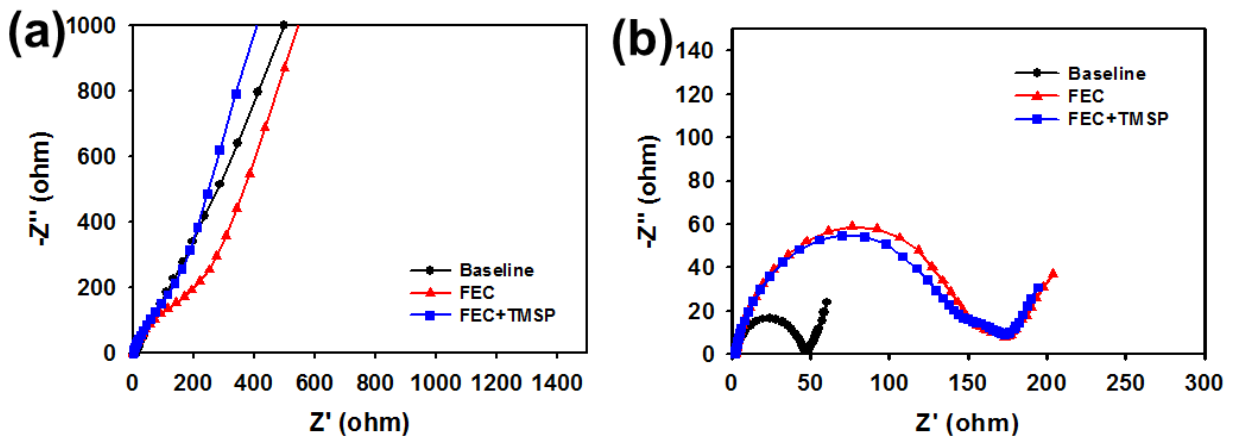
.

Figure 3-16. Electrochemical impedance spectra of Sn_4P_3 anodes (a) before and (b) after full sodiation in the baseline, FEC-added, and FEC+TMSP-added electrolyte

3-4 Conclusion

In summary, I demonstrate a FEC- and FEC+TMSP- containing electrolyte improves the cycling performance of Sn_4P_3. Especially, the FEC additive makes a resistive NaF-based SEI which prohibit the formation of $Na_{15}Sn_4$ phase with severe volume expansion. In TMSP additive cases, it effectively eliminated HF from the FEC decomposition to mitigate the formation of a large fraction of NaF and build up more stable and robust SEI layers. To identify possible mechanisms for formation of SEI, I proposed the surface chemistry on anode by using XPS and EDS data. In baseline electrolyte, carbonate and ether component on surface are detected. This component is derived by solvent decomposition due to volume expansion and ineffective SEI layer. However, the FEC- and FEC+TMSP-containing electrolytes reduce the solvent decomposition and made the stable SEI layers to prevent the aggregation of the Sn particles. Therefore, the results of this study and the associated analysis are expected to contribute to further development of advanced electrolytes for high performance metallic anodes for Na-ion batteries

Reference

1.   Tarascon, J. M.; Armand, M., Issues and challenges facing rechargeable lithium batteries. *Nature* **2001,** *414* (6861), 359-367.

2.   Dunn, B.; Kamath, H.; Tarascon, J. M., Electrical Energy Storage for the Grid: A Battery of Choices. *Science* **2011,** *334* (6058), 928-935.

3.   Etacheri, V.; Marom, R.; Elazari, R.; Salitra, G.; Aurbach, D., Challenges in the development of advanced Li-ion batteries: a review. *Energ Environ Sci* **2011,** *4* (9), 3243-3262.

4.   Choi, N. S.; Chen, Z. H.; Freunberger, S. A.; Ji, X. L.; Sun, Y. K.; Amine, K.; Yushin, G.; Nazar, L. F.; Cho, J.; Bruce, P. G., Challenges Facing Lithium Batteries and Electrical Double-Layer Capacitors. *Angew Chem Int Edit* **2012,** *51* (40), 9994-10024.

5.   Goodenough, J. B.; Park, K. S., The Li-Ion Rechargeable Battery: A Perspective. *J Am Chem Soc* **2013,** *135* (4), 1167-1176.

6.   Fang, T.; Duh, J. G.; Sheen, S. R., LiCoO2 cathode material coated with nano-crystallized ZnO for Li-ion batteries. *Thin Solid Films* **2004,** *469*, 361-365.

7.   Myung, S. T.; Kumagai, N.; Komaba, S.; Chung, H. T., Effects of Al doping on the microstructure of LiCoO2 cathode materials. *Solid State Ionics* **2001,** *139* (1-2), 47-56.

8.   Cho, J.; Kim, Y. J.; Park, B., Novel LiCoO2 cathode material with Al2O3 coating for a Li ion cell. *Chem Mater* **2000,** *12* (12), 3788-3791.

9.   Liu, L. J.; Wang, Z. X.; Li, H.; Chen, L. Q.; Huang, X. J., Al2O3-coated LiCoO2 as cathode material for lithium ion batteries. *Solid State Ionics* **2002,** *152*, 341-346.

10.   Gao, P. F.; Fu, J. W.; Yang, J.; Lv, R. G.; Wang, J. L.; Nuli, Y. N.; Tang, X. Z., Microporous carbon coated silicon core/shell nanocomposite via in situ polymerization for advanced Li-ion battery anode material. *Phys Chem Chem Phys* **2009,** *11* (47), 11101-11105.

11.   Zhao, Y.; Liu, X. Z.; Li, H. Q.; Zhai, T. Y.; Zhou, H. S., Hierarchical micro/nano porous

silicon Li-ion battery anodes. *Chem Commun* **2012,** *48* (42), 5079-5081.

12.   Koo, B.; Kim, H.; Cho, Y.; Lee, K. T.; Choi, N. S.; Cho, J., A Highly Cross-Linked Polymeric Binder for High-Performance Silicon Negative Electrodes in Lithium Ion Batteries. *Angew Chem Int Edit* **2012,** *51* (35), 8762-8767.

13.   Kim, C.; Jang, J. Y.; Choi, N. S.; Park, S., Multi-functionalities of natural polysaccharide for enhancing electrochemical performance of macroporous Si anodes. *Rsc Adv* **2014,** *4* (6), 3070-3074.

14.   Kovalenko, I.; Zdyrko, B.; Magasinski, A.; Hertzberg, B.; Milicev, Z.; Burtovyy, R.; Luzinov, I.; Yushin, G., A Major Constituent of Brown Algae for Use in High-Capacity Li-Ion Batteries. *Science* **2011,** *334* (6052), 75-79.

15.   Slater, M. D.; Kim, D.; Lee, E.; Johnson, C. S., Sodium-Ion Batteries. *Adv Funct Mater* **2013,** *23* (8), 947-958.

16.   Pan, H. L.; Hu, Y. S.; Chen, L. Q., Room-temperature stationary sodium-ion batteries for large-scale electric energy storage. *Energ Environ Sci* **2013,** *6* (8), 2338-2360.

17.   Palomares, V.; Serras, P.; Villaluenga, I.; Hueso, K. B.; Carretero-Gonzalez, J.; Rojo, T., Na-ion batteries, recent advances and present challenges to become low cost energy storage systems. *Energ Environ Sci* **2012,** *5* (3), 5884-5901.

18.   Kim, S. W.; Seo, D. H.; Ma, X. H.; Ceder, G.; Kang, K., Electrode Materials for Rechargeable Sodium-Ion Batteries: Potential Alternatives to Current Lithium-Ion Batteries. *Adv Energy Mater* **2012,** *2* (7), 710-721.

19.   Hong, S. Y.; Kim, Y.; Park, Y.; Choi, A.; Choi, N. S.; Lee, K. T., Charge carriers in rechargeable batteries: Na ions vs. Li ions. *Energ Environ Sci* **2013,** *6* (7), 2067-2081.

20.   Ponrouch, A.; Dedryvere, R.; Monti, D.; Demet, A. E.; Mba, J. M. A.; Croguennec, L.; Masquelier, C.; Johansson, P.; Palacin, M. R., Towards high energy density sodium ion batteries through electrolyte optimization. *Energ Environ Sci* **2013,** *6* (8), 2361-2369.

21.   Ponrouch, A.; Marchante, E.; Courty, M.; Tarascon, J. M.; Palacin, M. R., In search of an optimized electrolyte for Na-ion batteries. *Energ Environ Sci* **2012,** *5* (9), 8572-8583.

22.   Chen, L. B.; Wang, K.; Xie, X. H.; Xie, J. Y., Enhancing electrochemical performance of silicon film anode by vinylene carbonate electrolyte additive. *Electrochem Solid St* **2006,** *9* (11), A512-A515.

23.   Chen, L. B.; Wang, K.; Xie, X. H.; Xie, J. Y., Effect of vinylene carbonate (VC) as electrolyte additive on electrochemical performance of Si film anode for lithium ion batteries. *J Power Sources* **2007,** *174* (2), 538-543.

24.   Choi, N. S.; Yew, K. H.; Lee, K. Y.; Sung, M.; Kim, H.; Kim, S. S., Effect of fluoroethylene carbonate additive on interfacial properties of silicon thin-film electrode. *J Power Sources* **2006,** *161* (2), 1254-1259.

25.   Etacheri, V.; Haik, O.; Goffer, Y.; Roberts, G. A.; Stefan, I. C.; Fasching, R.; Aurbach, D., Effect of Fluoroethylene Carbonate (FEC) on the Performance and Surface Chemistry of Si-Nanowire Li-Ion Battery Anodes. *Langmuir* **2012,** *28* (1), 965-976.

26.   Han, G. B.; Ryou, M. H.; Cho, K. Y.; Lee, Y. M.; Park, J. K., Effect of succinic anhydride as an electrolyte additive on electrochemical characteristics of silicon thin-film electrode. *J Power Sources* **2010,** *195* (11), 3709-3714.

27.   Chun, M. J.; Park, H.; Park, S.; Choi, N. S., Bicontinuous structured silicon anode exhibiting stable cycling performance at elevated temperature. *Rsc Adv* **2013,** *3* (44), 21320-21325.

28.   Zhang, L. L.; Ma, Y. L.; Cheng, X. Q.; Zuo, P. J.; Cui, Y. Z.; Guan, T.; Du, C. Y.; Gao, Y. Z.; Yin, G. P., Enhancement of high voltage cycling performance and thermal stability of LiNi1/3Co1/3Mn1/3O2 cathode by use of boron-based additives. *Solid State Ionics* **2014,** *263*, 146-151.

29.   Ha, S. Y.; Han, J. G.; Song, Y. M.; Chun, M. J.; Han, S. I.; Shin, W. C.; Choi, N. S., Using a lithium bis(oxalato) borate additive to improve electrochemical performance of high-voltage spinel LiNi0.5Mn1.5O4 cathodes at 60 degrees C. *Electrochim Acta* **2013,** *104*, 170-177.

30.   Xiang, H. F.; Xu, H. Y.; Wang, Z. Z.; Chen, C. H., Dimethyl methylphosphonate (DMMP) as an efficient flame retardant additive for the lithium-ion battery electrolytes. *J Power Sources* **2007,**

173 (1), 562-564.

31.   Wang, Q. S.; Sun, J. H.; Yao, X. L.; Chen, C. H., 4-Isopropyl phenyl diphenyl phosphate as flame-retardant additive for lithium-ion battery electrolyte. *Electrochem Solid St* **2005,** *8* (9), A467-A470.

32.   Delmas, C.; Braconnier, J. J.; Fouassier, C.; Hagenmuller, P., Electrochemical Intercalation of Sodium in Naxcoo2 Bronzes. *Solid State Ionics* **1981,** *3-4* (Aug), 165-169.

33.   Shacklette, L. W.; Jow, T. R.; Townsend, L., Rechargeable Electrodes from Sodium Cobalt Bronzes. *J Electrochem Soc* **1988,** *135* (11), 2669-2674.

34.   Komaba, S.; Yabuuchi, N.; Nakayama, T.; Ogata, A.; Ishikawa, T.; Nakai, I., Study on the Reversible Electrode Reaction of Na1-xNi0.5Mn0.5O2 for a Rechargeable Sodium-Ion Battery. *Inorg Chem* **2012,** *51* (11), 6211-6220.

35.   Venkatraman, S.; Choi, J.; Manthiram, A., Factors influencing the chemical lithium extraction rate from layered LiNi1-y-zCoyMnzO2 cathodes. *Electrochem Commun* **2004,** *6* (8), 832-837.

36.   Kim, H.; Park, I.; Seo, D. H.; Lee, S.; Kim, S. W.; Kwon, W. J.; Park, Y. U.; Kim, C. S.; Jeon, S.; Kang, K., New Iron-Based Mixed-Polyanion Cathodes for Lithium and Sodium Rechargeable Batteries: Combined First Principles Calculations and Experimental Study. *J Am Chem Soc* **2012,** *134* (25), 10369-10372.

37.   Kim, H.; Park, I.; Lee, S.; Kim, H.; Park, K. Y.; Park, Y. U.; Kim, H.; Kim, J.; Lim, H. D.; Yoon, W. S.; Kang, K., Understanding the Electrochemical Mechanism of the New Iron-Based Mixed-Phosphate Na4Fe3(PO4)(2)(P2O7) in a Na Rechargeable Battery. *Chem Mater* **2013,** *25* (18), 3614-3622.

38.   Stevens, D. A.; Dahn, J. R., High capacity anode materials for rechargeable sodium-ion batteries. *J Electrochem Soc* **2000,** *147* (4), 1271-1273.

39.   Komaba, S.; Murata, W.; Ishikawa, T.; Yabuuchi, N.; Ozeki, T.; Nakayama, T.; Ogata, A.; Gotoh, K.; Fujiwara, K., Electrochemical Na Insertion and Solid Electrolyte Interphase for Hard-

Carbon Electrodes and Application to Na-Ion Batteries. *Adv Funct Mater* **2011,** *21* (20), 3859-3867.

40.   Datta, M. K.; Epur, R.; Saha, P.; Kadakia, K.; Park, S. K.; Kuma, P. N., Tin and graphite based nanocomposites: Potential anode for sodium ion batteries. *J Power Sources* **2013,** *225*, 316-322.

41.   Kim, Y.; Park, Y.; Choi, A.; Choi, N. S.; Kim, J.; Lee, J.; Ryu, J. H.; Oh, S. M.; Lee, K. T., An Amorphous Red Phosphorus/Carbon Composite as a Promising Anode Material for Sodium Ion Batteries. *Adv Mater* **2013,** *25* (22), 3045-3049.

42.   Qian, J. F.; Wu, X. Y.; Cao, Y. L.; Ai, X. P.; Yang, H. X., High Capacity and Rate Capability of Amorphous Phosphorus for Sodium Ion Batteries. *Angew Chem Int Edit* **2013,** *52* (17), 4633-4636.

43.   Qian, J. F.; Chen, Y.; Wu, L.; Cao, Y. L.; Ai, X. P.; Yang, H. X., High capacity Na-storage and superior cyclability of nanocomposite Sb/C anode for Na-ion batteries. *Chem Commun* **2012,** *48* (56), 7070-7072.

44.   Darwiche, A.; Marino, C.; Sougrati, M. T.; Fraisse, B.; Stievano, L.; Monconduit, L., Better Cycling Performances of Bulk Sb in Na-Ion Batteries Compared to Li-Ion Systems: An Unexpected Electrochemical Mechanism. *J Am Chem Soc* **2012,** *134* (51), 20805-20811.

45.   Zhou, X. S.; Dai, Z. H.; Bao, J. C.; Guo, Y. G., Wet milled synthesis of an Sb/MWCNT nanocomposite for improved sodium storage. *J Mater Chem A* **2013,** *1* (44), 13727-13731.

46.   Kim, Y.; Kim, Y.; Choi, A.; Woo, S.; Mok, D.; Choi, N. S.; Jung, Y. S.; Ryu, J. H.; Oh, S. M.; Lee, K. T., Tin Phosphide as a Promising Anode Material for Na-Ion Batteries. *Adv Mater* **2014,** *26* (24), 4139-4144.

47.   Li, W. J.; Chou, S. L.; Wang, J. Z.; Kim, J. H.; Liu, H. K.; Dou, S. X., Sn4+xP3 @ Amorphous Sn-P Composites as Anodes for Sodium-Ion Batteries with Low Cost, High Capacity, Long Life, and Superior Rate Capability. *Adv Mater* **2014,** *26* (24), 4037-4042.

48.   Qian, J. F.; Xiong, Y.; Cao, Y. L.; Ai, X. P.; Yang, H. X., Synergistic Na-Storage Reactions in Sn4P3 as a High-Capacity, Cycle-stable Anode of Na-Ion Batteries. *Nano Lett* **2014,** *14* (4), 1865-1869.

49.   Ellis, L. D.; Hatchard, T. D.; Obrovac, M. N., Reversible Insertion of Sodium in Tin. *J*

Electrochem Soc **2012,** *159* (11), A1801-A1805.

50.   Shen, Q.; Li, J. G.; Zhang, L. M., A study on Sn ion implantation into lead telluride thermoelectric material. *Sol Energ Mat Sol C* **2000,** *62* (1-2), 167-172.

51.   Majjane, A.; Chahine, A.; Et-tabirou, M.; Echchahed, B.; Do, T. O.; Mc Breen, P., X-ray photoelectron spectroscopy (XPS) and FTIR studies of vanadium barium phosphate glasses. *Mater Chem Phys* **2014,** *143* (2), 779-787.

52.   Ji, L. W.; Gu, M.; Shao, Y. Y.; Li, X. L.; Engelhard, M. H.; Arey, B. W.; Wang, W.; Nie, Z. M.; Xiao, J.; Wang, C. M.; Zhang, J. G.; Liu, J., Controlling SEI Formation on SnSb-Porous Carbon Nanofibers for Improved Na Ion Storage. *Adv Mater* **2014,** *26* (18), 2901-2908.